

This article was downloaded by: [Imperial College London Library]

On: 12 June 2015, At: 06:35

Publisher: Taylor & Francis

Informa Ltd Registered in England and Wales Registered Number: 1072954 Registered office: Mortimer House, 37-41 Mortimer Street, London W1T 3JH, UK



Combustion Science and Technology

Publication details, including instructions for authors and subscription information:

<http://www.tandfonline.com/loi/gcst20>

Turbulent Flamelet Propagation

J. C. VASSILICOS^a & J. C. R. HUNT^a

^a Department of Applied Mathematics and Theoretical Physics, University of Cambridge, Cambridge, U.K.

Published online: 27 Apr 2007.

To cite this article: J. C. VASSILICOS & J. C. R. HUNT (1993) Turbulent Flamelet Propagation, Combustion Science and Technology, 87:1-6, 291-327, DOI: [10.1080/00102209208947220](https://doi.org/10.1080/00102209208947220)

To link to this article: <http://dx.doi.org/10.1080/00102209208947220>

PLEASE SCROLL DOWN FOR ARTICLE

Taylor & Francis makes every effort to ensure the accuracy of all the information (the "Content") contained in the publications on our platform. However, Taylor & Francis, our agents, and our licensors make no representations or warranties whatsoever as to the accuracy, completeness, or suitability for any purpose of the Content. Any opinions and views expressed in this publication are the opinions and views of the authors, and are not the views of or endorsed by Taylor & Francis. The accuracy of the Content should not be relied upon and should be independently verified with primary sources of information. Taylor and Francis shall not be liable for any losses, actions, claims, proceedings, demands, costs, expenses, damages, and other liabilities whatsoever or howsoever caused arising directly or indirectly in connection with, in relation to or arising out of the use of the Content.

This article may be used for research, teaching, and private study purposes. Any substantial or systematic reproduction, redistribution, reselling, loan, sub-licensing, systematic supply, or distribution in any form to anyone is expressly forbidden. Terms & Conditions of access and use can be found at <http://www.tandfonline.com/page/terms-and-conditions>

Turbulent Flamelet Propagation

J. C. VASSILICOS and J. C. R. HUNT *Department of Applied Mathematics
and Theoretical Physics, University of Cambridge, Cambridge, U.K.*

(Received October 2, 1991; in revised form March 5, 1992)

Abstract—A formalism for a flamelet's evolution of its spatial distribution is derived from a field equation which is slightly more general than Williams' field equation. Unlike Williams' field equation, the field equation used here, though non-linear, has the property that an arbitrary linear combination of interface solutions (Heavyside type of functions) is also a solution. We therefore can describe the location of the flamelet with two interfaces rather than one, both moving relative to the flow in the same direction. The volume between these two interfaces is on average conserved; this makes it possible to define a probability density for the spatial distribution of the flamelet, and thereby derive equations describing the evolution of the spatial distribution of folds and wrinkles of the flame front.

Three main conclusions are reached in this paper using this formalism, through the exact analytical study of a flamelet in an arbitrary 1-d velocity field, and through the numerical study of a flamelet in a simulated 2-d turbulent velocity field.

(1) The rate of advancement u_M of the average location of the flame front can be smaller than the turbulent flame speed u_T at short times, and sometimes even smaller than the laminar flame speed u_L (at short times). It is shown, in the case of an arbitrary 1-d velocity field, that $u_M = u_T$ only after cusps have formed on the flamelet, and $u_M < u_L < u_T$ before.

(2) If the turbulence is too weak or too strong compared with the laminar flame speed, the dispersion of the flame is, at short times, increased by the turbulence and reduced by the laminar flame speed.

(3) The dispersion of the flame is skewed towards the direction of the flame's propagation at all times, even before cusp formation.

Key words: Flamelet, moving interfaces, flame speed, turbulence, field equation, cusps

1 INTRODUCTION

Turbulent combustion presents a plethora of different regimes with various phenomena and mechanisms appearing in each one of them. The complexity involved is enormous, and is the result of both the turbulence and the combustion and their interaction. Both introduce their own time and length scales (see, for example, Peters, 1987), and both are highly nonlinear, independently and in combination with each other.

In this paper we will be concerned with a very specific type of flame which is called the flamelet (see Peters, 1986). Such flames occur in premixed combustion, when the chemistry involved in the burning happens so fast that the flow has no time to influence the reaction-diffusion mechanism that is responsible for the propagation of the flamelet (see Calvin, 1985b). In other words, the ratio of the characteristic time of the chemistry (*i.e.*, the time it takes for the unburned reactants to be transformed into burned products) to any characteristic time of the velocity field is very small. In case the velocity field is turbulent, that means the Damkohler number (defined as the ratio of the turbulent time scale to the time scale of the chemistry) is large, and the Karlovitz number (defined as the ratio of the time scale of the chemistry to the turnover time t_K of the smallest turbulent eddies) is small. One can therefore decouple the thermochemistry from the turbulence, and even ignore it, in the sense that we can consider all the thermochemical information as being stored in only one parameter, the laminar flame speed u_L . That is an enormous simplification, as typically at least 300 different reactions are involved in combustion processes (see Clavin, 1985a), and

the calculation of u_L on those grounds becomes a formidable problem in itself. Here we will assume that problem solved, and the value of u_L given to us for a further study of the fluid dynamical aspect of flamelets. u_L is the speed with which a planar flame propagates in a fluid at rest as a result of the reaction–diffusion process, and is of course related to the characteristic time of the chemistry t_C by $u_L \sim (D/t_C)^{1/2}$, where D is the thermal diffusivity of the fluid.

One can also use the two basic quantities D and t_C involved in the reaction–diffusion process to estimate the thickness δ of the reaction zone, *i.e.*, the intermediary zone between burned and unburned fuel, where the chemical reactions are still under way. On physical and dimensional grounds one finds $\delta \sim (Dt_C)^{1/2}$.

Following experimental evidence (see, for example, Pope, 1987) one often assumes a Prandtl number Pr of unity in combusting flows, in which case a low Karlovitz number Ka implies that the thickness δ of the reaction zone is much smaller than any length scale of the turbulence, and in particular smaller than the Kolmogorov length scale $l_K \sim (\nu t_K)^{1/2}$ (ν is the kinematic viscosity). That follows directly from

$$\delta/l_K \sim \frac{(Dt_C)^{1/2}}{(\nu t_K)^{1/2}} \sim Ka^{1/2} Pr^{-1/2}.$$

For Prandtl numbers of order unity or larger, the flamelet is therefore essentially a flame sheet (see Pope, 1987) (“flamelet” and “flame sheet” are usually synonymous in the literature). It can be well described as a very thin interface separating burned from unburned fuel, convected, bent and strained by the turbulence (so that it is a highly wrinkled surface) and propagating normal to itself relative to the flow.

The intrinsic speed of propagation u_F of the flame sheet is not generally simply equal to u_L , but also depends on flame stretch which in turn depends on local properties on and around the flame sheet, like the curvature of the interface and the hydrodynamic rate of strain near it (Williams, 1985a). These are small effects, remnants of the influence of the velocity field on the thermochemistry and are of order δ/l_K at most. A good measure of the order of magnitude of the rate of strain is given by t_K^{-1} , which, because of the low value of Ka for flamelets ($t_K^{-1} \ll t_C^{-1}$), is small enough to influence the value of u_F to a much lesser extent than u_L does. u_F is indeed well approximated by u_L , particularly when the flame sheet is nearly planar, *i.e.*, when the flame sheet is weakly wrinkled and its curvature is everywhere small (see Calvin, 1985a; Williams, 1985a).

In order to ignore the effects that the flame can have on the turbulence, one further approximation is needed; neglect of velocity fluctuations caused by temperature differences and of thermal expansion. We therefore assume that both the density drop across the interface is too small to have any significant influence on the velocity field, and the viscosity—which is a function of temperature—remains constant over the flow. These are the conditions for the turbulence to influence the flame front without the flame front affecting the turbulence.

A simple field equation has been recently proposed to describe the motion of flame sheets where the dynamical effects of the small density and viscosity drops across the sheet can be neglected (Williams, 1985a, b). In the present chapter we are going to use a slightly more general variant of that field equation to derive the spatial statistics of the flame sheet; its average location, its spread, its asymmetry and properties characterising its propagation. Thus we will address the questions of how fast flame sheets move in terms of their laminar flame speed, how fast they deform and what the patterns of their deformation are. Williams’ field equation is in part identical to the advection equation that described the turbulent diffusion of a passive scalar. This

analogy will allow us to compare the spatial statistics of a flame sheet with those of a dispersing dye and draw some differences between a flame fronts' deformation and that of a simple material surface in turbulence. The methodology followed in this investigation is a combination of combustion and turbulent diffusion analysis.

The series of simplifying assumptions we made to bring the problem of the flamelet's behaviour down to Williams' equation exclude from this study a significant number of turbulent combustion phenomena, and in particular all known flame instabilities (see Sivashinsky, 1983). A large part of this chapter will be dealing with the short time behaviour of flamelets because Williams' equation usually breaks down for long enough times, after the appearance of singularities (*e.g.*, cusps) on the flamelet. That is precisely when instabilities may be expected to amplify; in case they do, this chapter's analysis and numerical results break down.

Our neglect of the density drop across the interface implies an absence of the Darrieus-Landau hydrodynamic instability, at least up to quite large wavelengths. It is indeed known that if one includes in u_f the small effect of flame stretch, then small wavelength disturbances are stabilised, and the smaller the density drop, the larger the critical wavelength of the stabilised disturbances (Markstein, 1951). If we set the Lewis number Le equal to 1 (*i.e.*, thermal and mass diffusivities are the same), thermodiffusive instabilities are out of the question too, and so the Markstein theory does indeed yield stabilisation of short wave disturbances (Sivashinsky, 1983).

The validity of this chapter's short time results is therefore limited to flamelets with $Le = 1$ that are small in extent compared to the critical wavelength above which disturbances are unstable.

In Section 2 we introduce Williams' equation and show how one can derive the spatial statistics of flamelets for short times. In Section 3 we briefly discuss and compare two different definitions of the turbulent flame speed. In Section 4 we study a 1-dimensional model problem and in Section 5 we present the results of 2-dimensional numerical simulations. One of the conclusions in Section 6 will be that the turbulent burning speed and the rate of advancement of the average location of the flamelet are not always equal.

Pope (1987) reports that "spark ignition engines and most laboratory experiments operate in the flame sheet regime".

2 SPATIAL STATISTICS OF FLAMELETS FOR SHORT TIMES

2.1 Williams' Equation

Williams (1985a, b) and others (Kerstein *et al.*, 1988; Sethian, 1985) pointed out recently that one can use a very simple field equation to describe a constant density (and constant viscosity) flame sheet. That equation, a variant of a classical result (Lamb, 1932, Chapter 1), is an advection equation. It states that a transported passive scalar field F is such that

$$F(\mathbf{x}_0, t_0) = F[\mathbf{x}(t, \mathbf{x}_0), t], \quad (2.1)$$

where $\mathbf{x}(t, \mathbf{x}_0)$ is the trajectory of the fluid element that was at \mathbf{x}_0 at time t_0 . If we chose to represent the flame sheet (in the limit of zero thickness) by a level surface $F = \text{Const.}$, then the trajectory of a "flame element" (it is not a fluid element!) is the result of both the local fluid velocity $\mathbf{u}(\mathbf{x}, t)$ and the self-propagation of the level

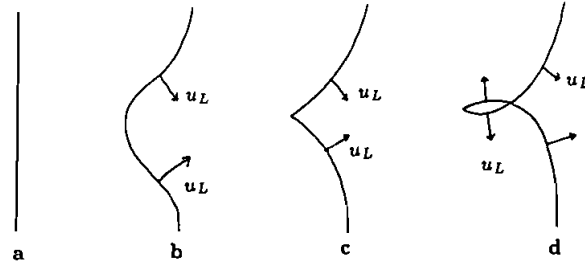


FIGURE 1. An initially plane flame interface (a) is bent by the velocity field (b) and then runs into itself because of its self-propagation normal to the surface. That produces a cusp (c). In a bad simulation of a flame sheet the cusp can degenerate into an expanding loop (d).

surface normal to itself with velocity u_F . In other words, in the limit $t \rightarrow t_0$,

$$\frac{\mathbf{x}(t, \mathbf{x}_0) - \mathbf{x}_0}{t - t_0} \approx \mathbf{u}(\mathbf{x}_0, t_0) + u_F \mathbf{n}(\mathbf{x}_0, t_0), \quad (2.2)$$

where $\mathbf{n}(\mathbf{x}, t)$ is the unit vector normal to the level surface $F = \text{Const.}$ that crosses the point \mathbf{x} at time t , and is oriented towards the “unburned” side of $F = \text{Const.}$ If F is a monotonic function along the direction \mathbf{n} , we can choose the “unburned” side to be towards the side of decreasing values of F , and therefore \mathbf{n} cannot be defined, *i.e.*, if F is not regular enough, and ∇F is either infinite or not unique in certain points of the flow. Pope (1988) has indeed shown how the regularity of self-propagating surfaces can break down, for example by the creation of cusps, which happens as a result of the surface running locally into itself after having been bent by the velocity field (see Figure 1). Cusps have been observed in experiments (*e.g.*, see Strehlov, 1984) and numerical computations (*e.g.*, Ashurst *et al.*, 1988; Osher and Sethian, 1988; Sethian, 1988). The present approach should therefore be considered valid before any cusp has had time to form.

A first order expansion of the right-hand side of Eq. (2.1) around $t = t_0$ and use of Eq. (2.2) gives

$$\frac{\partial}{\partial t} F + (\mathbf{u} + u_F \mathbf{n}) \cdot \nabla F = 0 \quad (2.3)$$

which becomes Williams’ equation if we replace \mathbf{n} by $-\nabla F/|\nabla F|$,

$$\frac{\partial}{\partial t} F + \mathbf{u} \cdot \nabla F = u_F |\nabla F|. \quad (2.4)$$

It is worth noting that Eqs. (2.3) and (2.4) are valid for both compressible and incompressible flows. These are not conservation equations but advection equations for a passive scalar. The passive scalar does not affect the velocity field and is conserved in its flight—see eq. (2.1). On the other hand, in compressible flows the density of a fluid particle is not conserved throughout the fluid particle’s flight; Define ρ to be the density of scalar F , so that

$$\rho = \frac{\delta F}{\delta V}, \quad (2.5)$$

where δV is the infinitesimal volume of the fluid particle carrying the infinitesimal scalar quantity δF , which is also a passive scalar transported according to eqs. (2.3) and (2.4). We can now write down the following conservation equation:

$$\frac{\partial}{\partial t} \rho + \nabla \cdot (\mathbf{u} + u_f \mathbf{n}) \rho = 0 \quad (2.6)$$

which can be deduced in the usual way (see Batchelor, 1967, Chapter 2) from the conservation of the global quantity $\int \rho \, dV$. Only if the flow is incompressible can Eq. (2.6) be rewritten in the form (assuming also u_f to be independent of space, *i.e.*, $u_f = u_L$)

$$\frac{\partial}{\partial t} \rho + \mathbf{u} \cdot \nabla \rho = u_L \nabla \cdot \rho \mathbf{n}. \quad (2.7)$$

The right-hand side ‘‘source’’ term in Eq. (2.7) originates from the contraction or expansion of δV due to the self-propagation of isoscalar surfaces. (Note that the left-hand side of Eq. (2.7) is not identically 0 for an incompressible flow unless $u_L = 0$.) Indeed from Eq. (2.3) (written for δF and not for F) and Eq. (2.6) we can deduce

$$\frac{dV}{dt} = \delta V \nabla \cdot (\mathbf{u} + u_f \mathbf{n}), \quad (2.8)$$

which is also a variant of another well known classical result (Batchelor, 1967, Chapter 3). For incompressible flows (and $u_f = u_L$) Eq. (2.8) becomes

$$\frac{d\delta V}{dt} = \delta V u_L \nabla \cdot \mathbf{n}. \quad (2.9)$$

Cusps form at those points of the interface where δV tends to zero (see Figure 1). In fact, $\nabla \cdot \mathbf{n} = K_1 + K_2$ (where K_1 and K_2 are the two principal curvatures on a given point of the level surface $F = \text{Const.}$), and cusps appear (by definition) at those points where one of the two principal curvatures becomes infinite (that is also the only way, as one can clearly see in Eq. (2.9), for δV to become zero in finite time). If we define K to be a characteristic value (in case there is one) of the curvature on the surface, then it is clear from a simple dimensional argument that the time t_{cusp} needed for a cusp to form is of the order (and in general, smaller than)

$$t_{\text{cusp}} \sim (K u_L)^{-1}. \quad (2.10)$$

Clearly, the validity of Eqs. (2.2)–(2.9), and in particular Eqs (2.3), (2.4) and their consequences, will be restricted to times $t \ll t_{\text{cusp}}$. In Pope (1988) one can find a general evolution equation for K_1 and K_2 whereby it can be shown that K_1 (or K_2) will remain finite for all finite times, if u_f goes to zero at least as rapidly as K_1^{-1} (or K_2^{-1}), or if the action of turbulent straining is fast enough (it has in fact been suggested that this does occur in some turbulent premixed flames, see Williams, 1985a). The order of magnitude of an appropriately defined value of K (let alone its precise value), has not yet been clarified; so at this stage, we can only say that Eq. (2.10) provides an estimate for the time (and length scale) validity of the present study.

It has been realised recently that a formalism based on Eq. (2.4) can have a number

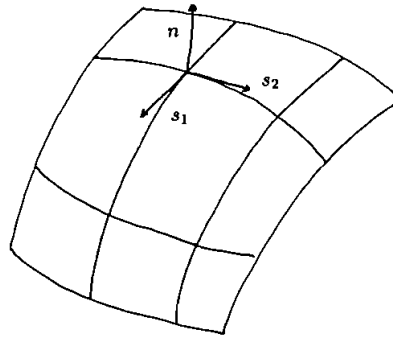


FIGURE 2 Parametric representation of the interface; s_1 and s_2 are the two components along two directions tangent to the interface at a given point of the interface, and orthogonal to each other; n is the component along the normal to the interface at that same point. As long as it is smooth, the interface can be defined by a relation $n = v(s_1, s_2, t)$ at all times before any irregularities form.

of advantages for both a computational and an analytical study of flame propagation. Initial value problems have been solved numerically for several configurations and flows (Osher and Sethian, 1988; Ashurst *et al.*, 1988). Kerstein *et al.* (1988) have derived from Eq. (2.4) an expression for the turbulent burning speed that is a volume averaged functional of the evolving scalar field F . That allows one to compute the turbulent burning speed numerically, without having to track a single interface within the Eulerian computational domain. Yakhot (1988) has also derived a formula for the turbulent burning speed as a function of the laminar flame speed and the turbulent velocity fluctuations, by applying dynamic renormalisation group analysis to Eq. (2.4). An alternative renormalisation group approach to Eq. (2.4) has led to a description of the “bending” effect (Sivashinsky, 1988). Furthermore, starting from that same evolution Eq. (2.4), Peters *et al.* (1988) have attempted to obtain a semi-empirical model equation for the flame surface area.

The problem we are proposing to deal with here is the following: given the statistics of the turbulent velocity field $u(x, t)$, how can one extract from Eq. (2.3) or Eq. (2.4) the spatial statistics of the entire flame interface? (Pope (1988) has derived equations for spatial properties—*e.g.*, curvature, normal and tangents—of *infinitesimal surface elements*, and therefore his approach is *local*, whereas the present approach is *global*, *i.e.*, valid for the *entire* flamelet interface).

2.2 Interface Solutions of Williams' Equation

Let us start with the remark that if at time $t = 0$, $F(x, t = 0)$ is a Heaviside type of function, then at any time t later, the solution $F(x, t)$ of Eq. (2.3) or Eq. (2.4) is still a Heaviside type of function. Formally this means that

$$F(s_1, s_2, n; t) = H [n - v(s_1, s_2, t)] \quad (2.11)$$

is a solution of Eq. (2.3) or of Eq. (2.4). H is the Heaviside function, n , s_1 and s_2 are local coordinates on the interface defining the separation between regions where $F = 1$ and regions where $F = 0$ (see Figure 2), and $n = v(s_1, s_2, t)$ is the parametric relation defining the interface at time t (see Appendix A). Equation (2.11) is valid for as long as the interface does not intersect itself (*i.e.*, $v(s_1, s_2, t)$ is single valued).

In Appendix A we take this result one step further; we prove that any linear combination of such step functions is also solution of Eq. (2.3) but not of Eq. (2.4).

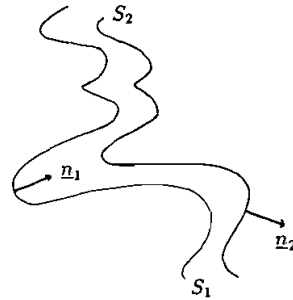


FIGURE 3 Two interfaces S_1 and S_2 . $F_i = 1$ behind and $F_i = 0$ in front of S_i , $i = 1, 2$. $f = F_2 - F_1$ is equal to 1 in the region between S_1 and S_2 and 0 everywhere else. V in (2.14) is the volume of this region.

Equation (2.3) is indeed more general than Eq. (2.4), so that any solution of Eq. (2.4) is also solution of Eq. (2.3) but the converse is not true. Equation (2.4) has been deduced from Eq. (2.3) under the assumption that F is a monotonic function of n . For example, f as defined in Eq. (2.12) is not such a function and is a solution of Eq. (2.3) but not of Eq. (2.4).

Note that even though Eq. (2.3) is a non-linear equation, there exists a set of solutions [of the form (2.11)] of which linear combinations are also solutions of Eq. (2.3).

In the sequel, we are going to focus our attention on a particular linear combination of such step functions (see Figure 3):

$$f = F_2 - F_1, \quad (2.12)$$

where

$$F_{1,2} = H [n - v_{1,2}(s_1, s_2, t)], \quad (2.13a)$$

with

$$v_2(s_1, s_2, t) > v_1(s_1, s_2, t). \quad (2.13b)$$

Inequality (2.13b) is crucial if we want f to be solution of the field equation (2.3). It states that the two interfaces defined by F_1 and F_2 do not intersect. That does not hold true in general for long enough times (Pope, 1988), in which case the present analysis breaks down.

The second interface (defined by F_2) is no more than a mere mathematical artifact. It has no physical significance. Whilst the first interface (defined by F_1) can be thought of as the actual interface between burnt and unburnt fuel, the surface related to F_2 is a “ghost” surface that is defined in order to develop an alternative kinematic analysis of the flame front. The advantage of this analysis is that it focuses on a function f that is non-zero only in the neighborhood of the flame sheet, as opposed to a function F_1 or F_2 that is non-vanishing on one of the two sides of the front. The fact (as we show in the next section) that the region where $f = 1$ has on average a constant volume in time (average over realisations), allows us to interpret the ratio of an average value of f to that average volume as being a probability density describing the spatial distribution of the front. This leads to a derivation from Eq. (2.3) of equations describing the evolution of the averaged spatial moments of the front.

2.3 Conservation of the Volume Between Two Fronts

What we define to be the volume V between two fronts is the volume between interfaces 1 and 2 (see Figure 3):

$$V = \int_{\text{all space}} f dV \quad (2.14)$$

From Eq. (2.3) it follows that:

$$\frac{dV}{dt} = - \int_{\text{all space}} (\mathbf{u} + u_F \mathbf{n}) \cdot \nabla f dV. \quad (2.15)$$

Assuming the turbulent flow $\mathbf{u}(\mathbf{x}, t)$ to be incompressible, and $u_F = u_L$ (i.e., u_F is independent of space), one is left with:

$$\frac{dV}{dt} = u_L \int_{\text{all space}} (\mathbf{n}_2 \cdot \nabla F_2 - \mathbf{n}_1 \cdot \nabla F_1) dV \quad (2.16)$$

(see Figure 3 for definitions of \mathbf{n}_1 and \mathbf{n}_2) Hence:

$$\frac{dV}{dt} = u_L \int_{\text{all space}} (|\nabla F_2| - |\nabla F_1|) dV. \quad (2.17)$$

Since, from Eq. (B.2) in Appendix B:

$$\int_{\text{all space}} |\nabla F_{1,2}| dV = A_{1,2}, \quad (2.18)$$

where A_i , ($i = 1, 2$) is the surface area of the interface S_i (see Figure 3), Eq. (2.17) becomes

$$\frac{dV}{dt} = u_L (A_2 - A_1). \quad (2.19)$$

This is an exact result valid for any particular realisation of the flow field. Define \bar{V} to be the average volume between two fronts over a large number of realisations, and \bar{A}_i the average surface area of interface S_i . If the velocity field $\mathbf{u}(\mathbf{x}, t)$ is homogeneous and isotropic, then one can safely assume that:

$$\bar{A}_2 = \bar{A}_1, \quad (2.20)$$

and hence derive the statistical conservation of the volume between two fronts.

$$\frac{d\bar{V}}{dt} = 0. \quad (2.21)$$

2.4 Time Evolution of the Spatial Moments

Probability theory has established that all the moments of a distribution determine the distribution itself. The spatial moments of f are defined as follows:

$$I_\alpha^q = \int_{\text{all space}} x_\alpha^q f dV \quad (2.22)$$

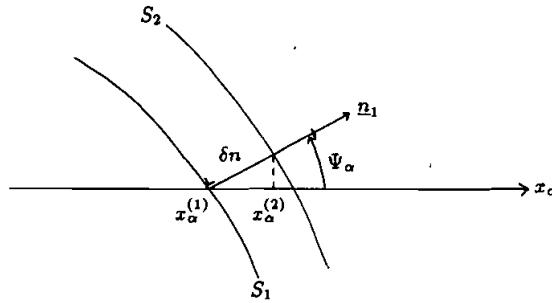


FIGURE 4 An axis generically described by x_α cuts S_1 at a point of coordinate $x_\alpha^{(1)}$ along that axis. Ψ_α is the angle that the normal to S_1 on that point makes with the α -axis, and δn is the infinitesimal distance between S_1 and S_2 along that normal. That normal cuts S_2 at a point of α -coordinate $x_\alpha^{(2)}$.

—for $\alpha = 1, 2, 3$ —and use Eq. (2.3) to obtain their evolution equation:

$$\dot{I}_\alpha^q = - \int_{\text{all space}} x_\alpha^q (\mathbf{u} + u_f \mathbf{n}) \cdot \nabla f \, dV \quad (2.23)$$

Using the incompressibility condition and setting $u_f = u_L$ one gets

$$\dot{I}_\alpha^q = u_L \int_{\text{all space}} x_\alpha^q (|\nabla F_2| - |\nabla F_1|) \, dV + q \int_V u_\alpha x_\alpha^{q-1} \, dV \quad (2.24)$$

and recalling formula (B.3), we obtain the following result:

$$\dot{I}_\alpha^q = u_L \left[\int_{S_2} x_\alpha^q \, dS - \int_{S_1} x_\alpha^q \, dS \right] + q \int_V u_\alpha x_\alpha^{q-1} \, dV \quad (2.25)$$

(Integrals over the volume V are taken over the space where $f = 1$ —see (2.14).)

Until now, all our calculations (and in particular Eqs (2.21) and (2.25)) have been valid for “interface widths” (that is the distance between interfaces S_1 and S_2) of any size. The only restriction to their validity—besides $u_f = u_L$ and the homogeneity, isotropy and incompressibility of $\mathbf{u}(x, t)$ —has been that this “interface width” is nowhere equal to zero, *i.e.*, that S_1 and S_2 do not intersect.

Let us see what happens to Eq. (2.25) when the two interfaces S_1 and S_2 are close together. One ought to keep in mind of course, that the closer the distance δn between those interfaces, the shorter in time the validity of our results will be. Then the x_α coordinates of the two interfaces S_1 and S_2 are related to δn by (see Figure 4):

$$x_\alpha^{(2)} = x_\alpha^{(1)} + \delta n \cos \Psi_\alpha. \quad (2.26)$$

Therefore,

$$\int_{S_2} x_\alpha^{(2)q} \, dS \approx \int_{S_1} x_\alpha^{(1)q} \, dS + q \int_{S_1} \delta n \cos \Psi_\alpha x_\alpha^{(1)(q-1)} \, dS. \quad (2.27)$$

Thus, one is finally left with:

$$\frac{d}{dt} I_\alpha^q = qu_L \int_{S_1} \delta n \cos \Psi_\alpha x_\alpha^{q-1} \, dS + q \int_V u_\alpha x_\alpha^{q-1} \, dV. \quad (2.28)$$

This result provides the means of relating the statistics of the flame front [(left-hand side of Eq. (2.28)] to the relative importance of the flame velocity [first term on the right-hand side of (2.28)] and the turbulent diffusion [second term on the right-hand side of (2.28)]. This dichotomy is of course a bit arbitrary, as both terms are really “mixed”, in the sense that the shapes of the surface S_1 and the volume V are determined from both the turbulent velocity field \mathbf{u} and the combustion u_L . Note that we would not have been able to derive it without the use of two interfaces rather than one!

2.5 The Lower Order Averaged Spatial Moments

The three lower order spatial moments, and their time derivatives as obtained in Eq. (2.28) are particularly interesting because of their clear physical interpretation.

$$X_\alpha \equiv \frac{1}{\bar{V}} \overline{I_\alpha^1} = \frac{1}{\bar{V}} \overline{\int_{\text{all space}} x_\alpha f dV} \quad (2.29)$$

determines the mean location of the flame, and therefore defines the mean transport. (The overbar signifies an average over a large number of realisations of the flow.) A combination of X_α and the second order moment I_α^{22} gives a measure of the dispersion Δ_α^2 of the flame front, or the width of the interface distortions:

$$\Delta_\alpha^2 \equiv \frac{1}{\bar{V}} \overline{\int_{\text{all space}} (x_\alpha - X_\alpha)^2 f dV} = \frac{\overline{I_\alpha^2}}{\bar{V}} - X_\alpha^2. \quad (2.30)$$

And finally, the skewness

$$\Sigma_\alpha \equiv \frac{1}{\bar{V}} \overline{\int_{\text{all space}} (x_\alpha - X_\alpha)^3 f dV} = \frac{\overline{I_\alpha^3}}{\bar{V}} - X_\alpha^3 - 3X_\alpha \Delta_\alpha^2 \quad (2.31)$$

accounts for any statistical asymmetry in the shape of the flame about its mean position X_α .

Let us start with X_α . Under the additional assumptions that the mean turbulent velocity is zero—which actually follows from the isotropy of the turbulence—and that the interface samples the uniformly, or if the turbulence intensity is weak compared to u_L , one can neglect $\int_V u_\alpha dV$, and Eq. (2.28) takes the following simple form:

$$\dot{X}_\alpha \approx \frac{u_L}{\bar{V}} \overline{\int_{S_1} \delta n \cos \Psi_\alpha dS}. \quad (2.32)$$

That makes perfect sense, because the average location of the flame does indeed change only as a result of the combustion. It is well known that homogeneous and isotropic turbulence does not affect the mean position of a passively advected interface.

Equation (2.32) provides an expression for the mean speed \dot{X}_α of the flame in the α -direction. Notice that for the trivial case of a plane flame front, Eq. (2.32) gives

$$\dot{X}_\alpha = u_L \frac{\delta n S_1}{\delta n S_1} = u_L \quad (2.33)$$

as expected. Since $\cos \Psi_\alpha \leq 1$, it also becomes clear that

$$\dot{X}_\alpha \leq u_L. \quad (2.34)$$

In other words the fluctuations of the interface due to the turbulence reduce the mean speed of the flame front. So, even though the turbulence does not directly cause the flame to advance on the average, it does slow down the average advancement due to combustion! (We have neglected the effect of flame stretch, which may have a competing effect and tend to accelerate the average advancement of the flamelet.) One should be careful not to mistake \dot{X}_s for the turbulent burning speed, which is defined as a surface to volume ratio, and which increases with the turbulence because the area of the flame front does. The difference between these two speeds (which are often confused) will turn out (in Section 3) to be a consequence of the non-vanishing value of the skewness Σ_α .

We now focus on the dispersion of the flame front. Using Eq. (2.28) for $q = 1$ and $q = 2$, we obtain the rate of growth of the mean square dispersion:

$$\frac{d}{dt} \Delta_\alpha^2 = \frac{2u_L}{\bar{V}} \int_{S_1} \delta n \cos \Psi_\alpha(x_\alpha - X_\alpha) dS + \frac{2}{\bar{V}} \int_V u_\alpha(x_\alpha - X_\alpha) dV. \quad (2.35)$$

Setting $u_L = 0$, it yields Taylor's result for the mean square dispersion of a sheet in a turbulent flow (Taylor, 1921) (provided $u_\alpha = 0$):

$$\Delta_\alpha^2 = 2 \int_0^t \langle \overline{u_\alpha x_\alpha} \rangle d\tau + \text{Const.}, \quad (2.36)$$

where the brackets signify an average over space. Then restore $u_L \neq 0$, and notice that the "combustion term" of Eq. (2.35) (the first term of the right-hand side) tends to increase the rate of growth of the mean square dispersion; but the surface growth of the interface may be slower as u_L increases thus reducing the domain of integration of the second term of the right-hand side of Eq. (2.35), and therefore acting to reduce $d/dt \Delta_\alpha^2$. Whether the overall effect is one of reduction or increase is not a trivial question. In Section 5 we present the results of a numerical simulation of a moving line-interface in a 2-dimensional turbulent velocity field and we find that for small times Δ_α^2 has a smaller value when $u_L \neq 0$ than when $u_L = 0$. One may indeed expect by direct inspection of Eq. (2.35) that this should be the case when the turbulence intensity is weak in comparison with u_L (as the numerical experiment of Section 5 corroborates) or when u_L is slightly non-vanishing and much smaller than the turbulent intensity.

That conclusion is to be contrasted with another by Townsend (see Batchelor and Townsend, 1956) where he showed that for very short times, molecular diffusion increases the turbulent dispersion of a passive scalar in a turbulent velocity field. Then as time increases slightly for second order effects in time to be significant, Saffman (1960) has shown that there is an interaction between turbulent and molecular diffusion that reduces the dispersion of that passive quantity or substance. Finally for large times, molecular diffusion and turbulent dispersion have cumulative effects.

One can speculate that a similar effect to that of Saffman's could sometimes happen to the dispersion of a flame sheet for all times. In certain situations (Ashurst *et al.*, 1988; Peters, 1986), the flame sheet develops cusps after a short period of time. As argued by Moffatt (1987), the structure of the flame front will be dominated by cusps below the Gibson scale. (In the flamelet regime Peters (1986) has argued that there exists a lower cut-off scale—the Gibson scale—below which the flame will not be significantly wrinkled.) These cusps should therefore decrease the range of scales where violent contortions of the flame occur, thereby reducing the overall dispersion of the flame sheet.

Seen that way, this mechanism is comparable to the one by which molecular diffusion reduces the dispersion of a passive scalar with low Prandtl number. Molecular diffusion smears off small scale distortions of isoscalar surfaces and therefore decreases the range of scales in which scalar fluctuations occur, which in turn decreases the magnitude of scalar fluctuations.

The scale below which fluctuations are smeared off is the Batchelor length scale (Batchelor, 1959), which is larger than the Kolmogorov length scale at low Prandtl numbers.

There is therefore a parallel between that Batchelor scale and the Gibson scale. According to Peters (1986) the Gibson scale exists only if u_L is significantly larger than the characteristic velocity of the smallest eddies of the turbulence, which is the condition for the Gibson scale to be larger than the Kolmogorov scale.

Equation (2.3) and the interface solutions (A.6) to this equation are only valid for times much shorter than the times needed for cusps to form on the flame sheet. It is therefore impossible to reach, in our present analysis, the effects we just described.

Let us now move to the third order spatial moment. Using Eq. (2.28) for $q = 1, 2, 3$ to calculate the time derivative of Eq. (2.31), we get:

$$\dot{\Sigma}_\alpha = \frac{3u_L}{\bar{V}} \int_{S_1} \overline{\delta n \cos \Psi_\alpha [(x_\alpha - X_\alpha)^2 - \Delta_\alpha^2]} dS + \frac{3}{\bar{V}} \int_V \overline{u_\alpha [(x_\alpha - X_\alpha)^2 - \Delta_\alpha^2]} dV \quad (2.37)$$

In case $u_L = 0$, the average over space, and the average over a large number of realisations commute, so that the overbar in Eq. (2.30) can be omitted, and one is left with

$$\dot{\Sigma}_\alpha = \frac{3}{\bar{V}} \int_V \bar{u}_\alpha (x_\alpha - X_\alpha)^2 dV - \frac{3}{\bar{V}} \int_V \bar{u}_\alpha dV \frac{1}{\bar{V}} \int_V (x_\alpha - X_\alpha)^2 dV \quad (2.38)$$

which vanishes when $\bar{u}_\alpha = 0$, and so it is clear that in general $\dot{\Sigma}_\alpha \neq 0$ only if $u_L \neq 0$. It is therefore the laminar flame speed that is entirely responsible for the development of asymmetry in the interface. That is shown here to happen for very short times, much shorter than the times needed for the flame sheet to develop cusps (as a surface propagating normal to itself is known to do in certain circumstances); but that is consistent with this cusp formation which causes the interface to be skewed at a further stage of the flame's evolution. One can also suspect that in general Σ_α will have the same sign as u_L , thus indicating that the dispersion of the flame front is skewed towards the direction of the flame's propagation. That is corroborated by the numerical simulations in Section 5.

3 WHAT IS THE TURBULENT FLAME SPEED?

It is usually assumed that the turbulent burning speed u_T is the same as the speed u_M with which the average location of the flame front advances. Recent renormalisation group analysis of flame sheets based on William's Eq. (2.4) by Yakhot (1988) or by Sivashinsky (1988) have been based on such an assumption. The intuitive idea is that if one stands far enough from the turbulent flame to be unable to resolve its wrinkles, one should still be able to measure how fast the fuel burns. And furthermore, u_M , the speed with which this average flame front, now "laminar", advances, can be nothing else but this rate of burning, *i.e.*, $u_M = u_T$. The trouble with such a reasoning is that

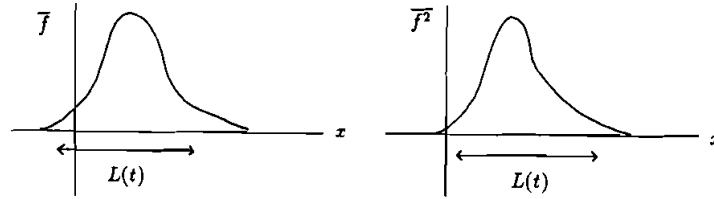


FIGURE 5 The distribution of the mean moments $\bar{f}, \bar{f}^2, \dots$ in space (e.g. along the x -coordinate), and the length scale $L(t)$ that characterises their width (variance).

it only holds provided the distribution of folds and deformations of the flamelet is symmetric about its mean position. As we have shown in the previous section, for small times, the distribution of folds is skewed towards the unburned side of the average position of the flamelet, and the appearance of cusps in finite time suggests that the distribution of folds may often remain skewed towards the direction of the flamelet's self-propagation. The total volume of fuel burned \mathbb{V} will therefore be larger than the volume of fuel V_M lying on the "burned side" of the average position of the flame. In fact, if V_B is the volume of burned fuel on the unburned side of the average position of the flame and V_U the volume of unburned fuel on the burned side of the average position of the flame (see Figure 7), then

$$\mathbb{V} = V_M + V_B - V_U. \tag{3.1}$$

The asymmetry of the interface towards the direction of flame propagation indicates that $V_B > V_U$ (see Figure 7), and therefore $V_T > V_M$. Because initially $\mathbb{V} = V_M$, the only way this can be achieved is for u_T to be larger than $u\delta_M$ at least for short times.

If α is chosen to indicate the direction in which the average position of the flame front advances, then

$$u_M = \frac{d}{dt} \left(\frac{1}{V} I_\alpha' \right)$$

(we could have also defined $u_M = \dot{X}_\alpha$, but it is not necessary to include averages over realisations in this section's analysis as it would remain essentially the same) and using

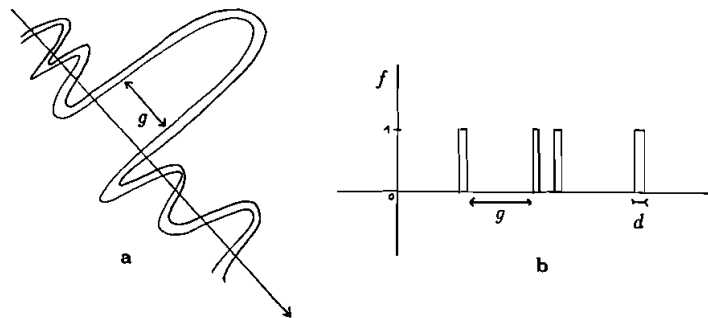


FIGURE 6 a) A cut through a front described by a double interface. b) The function f along this cut. It is equal to 1 between the interfaces; d is a characteristic (average) width of the distance between these interfaces, and g is the characteristic (average) width of the folds (gap between two crossovers of the front along the cut).

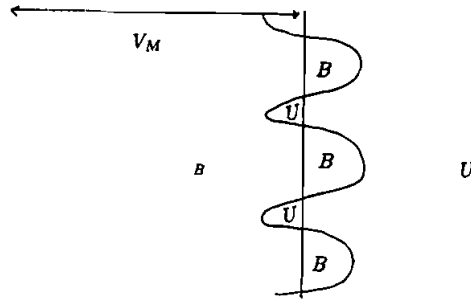


FIGURE 7. A curved interface representing a flame with B written on the burned side and U written on the unburned side. The average position of the interface is represented by a vertical straight line cutting through the curved interface, and V_M is the volume behind it (towards the burned side). V_B is the volume of the regions on the right hand side and V_U is the volume of the regions on the left hand side of the average position of the flame.

Eq. (2.28) for $q = 1$ we obtain:

$$u_M \approx \frac{1}{V} \int_S \delta n u_L \cos \Psi_\alpha dS + \frac{1}{V} \int_V u_x dV, \quad (3.2)$$

where we have replaced S for S_1 and ignored the extra term proportional to \dot{V} because we will take the limit $\delta n \rightarrow 0$, in which case it is clear from Eq. (2.19) that $\dot{V} \rightarrow 0$. If A is the area of the surface S , then at the limit $\delta n \rightarrow 0$, $V \approx A \delta n$ and Eq. (3.2) takes the following simpler form:

$$u_M = \frac{1}{A} \int_S (u_L \cos \Psi_\alpha + u_x) dS. \quad (3.3)$$

Formula (3.3) is intuitively obvious; it represents the weighted average of the velocity ($u_L \cos \Psi_\alpha + u_x$) with which each point on the surface moves along the direction α . One could have started this section by simply stating it as a sound definition of u_M for flamelets, rather than using Eq. (2.3) to derive it for short times. On the other hand, having derived it that way stresses the fact that Eq. (3.3) may not be valid any further as time progresses, and indeed, as we shall see in Section 4, as soon as cusps form on the interface (and \mathbf{n} cannot be defined in some points of the surface) Eq. (3.3) does not hold anymore.

The most common and conventional definition of the turbulent burning speed u_T of a flamelet is that of an area to volume ratio (Damkohler, 1941). That is the area of the flamelet's surface per unit volume. That definition is formally equivalent to

$$u_T(t) = u_L \frac{A(t)}{A_0}, \quad (3.4)$$

where $A(t)$ is the area of the interface (or of a sample of the interface) at time t , and $A_0 = A(t = 0)$. $u_L A(t)$ is the rate of volume burned, and A_0 is a normalisation factor so that u_T and u_L have the same dimensions and be comparable. (The area to volume ratio would be $A(t)/A_0 l_0$, where l_0 is chosen so that the area $A(t)$ be contained in a box of volume $A_0 l_0$, and is essentially the same as in Eq. (3.4) but in different units.)

It is interesting to note that even though it is geometrically evident that

$$u_L \dot{A}(t) = \frac{dV}{dt} \quad (3.5)$$

is the rate of volume \mathbb{V} burned, one can also deduce Eq. (3.5) from Eq. (2.3) or Eq. (2.4). The calculation runs exactly as in Section 2.3 which led to a similar formula (2.19), but with a different choice of a special discontinuous solution f of Eq. (2.3), this time $f' = F_1$, which is also solution of Eq. (2.4). In that case, $\mathbb{V} = \int f' dV$ and $A = \int |\nabla f'| dV$, and Eq. (3.5) is simply a matter of integrating both sides of Eq. (2.4) over the whole space.

Kerstein *et al.* (1988) have derived a result which in fact is a generalisation of Eq. (3.4). They have shown that any *continuous* solution g of Eq. (2.4) can also be used to compute the turbulent burning speed of the flame sheet (in which case the flame sheet is an isosurface $g = \text{Const.}$, and g has the dimensions of a length). They obtain the following formula:

$$u_T = u_L \langle |\nabla g| \rangle, \quad (3.6)$$

where the brackets denote an average of space, *i.e.*

$$\langle |\nabla g| \rangle = \frac{1}{\mathbb{V}_\infty} \int_{\mathbb{V}_\infty} |\nabla g| dV$$

(\mathbb{V}_∞ is the volume of all available space). Notice that if one arbitrarily replaces g by $f' = F_1$ in the right-hand side of Eq. (3.6) one essentially recovers Eq. (3.4).

The straining motions in turbulent flows produce an exponential growth of the area $A(t)$ (Batchelor, 1952; Drummond and Munch, 1990). Thus the turbulence enhances u_T and the combustion dramatically.

u_M 's dependence on $A(t)$ can be easily derived for short times from Eq. (3.3);

$$u_M(t) = u_L \frac{A_0^\alpha}{A(t)} + \frac{1}{A(t)} \int_S u_\alpha dS, \quad (3.7)$$

where $A_0^\alpha = \int_S \cos \Psi_\alpha dS$ is the area of the projection of S on the plane orthogonal to the direction α . If that plane coincides with the initial configuration of the flame interface, then $A_0^\alpha = A_0$.

Let us now assume the velocity field $\mathbf{u}(\mathbf{x}, t)$ is turbulent and such that $\langle \mathbf{u} \rangle = 0$.

In case the surface S has had time to sample the flow uniformly before the validity of Eq. (3.3) breaks down (which may happen if the turbulent intensity $\langle u^2 \rangle^{1/2}$ is much larger than u_L), or if $\langle u^2 \rangle^{1/2}$ is much smaller than u_L , one can approximately write (with the suitable choice of direction α):

$$u_M(t) \approx u_L \frac{A_0}{A(t)}, \quad (3.8)$$

which is essentially the same as Eq. (2.32), and therefore in agreement with inequality (2.34).

In the first case of very strong turbulence intensity this suggests an initial decay of u_M below u_L . The average location of the flamelet starts off by decelerating, increasingly so for increasingly strong turbulence and for increasingly fast burning. This enhanced burning is due to the enormous extent of the contortions of the interface about its average location, which seems to grow initially much faster than the flamelet's average location advances ($u_M \ll u_L \ll u_T$).

In the case of weak turbulence, $A(t)$ will start growing slightly above A_0 , and so u_M will be smaller than u_L but not too small and $u_L \ll u_T$. The flamelet is now a little

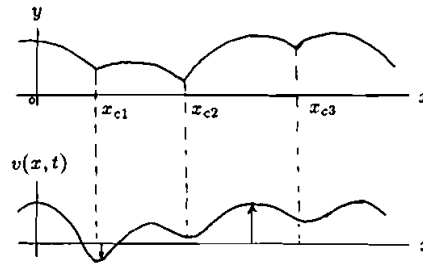


FIGURE 8 The 1-dimensional velocity field $v(x, t)$, and the flame interface as it looks after all possible cusps have formed. The flamelet is initially at $y = 0$, and x_{c_j} ($j = 1, 2, 3, \dots$) are the x -coordinates of the cusps on the flamelet. They correspond to the local minima of the velocity field.

wrinkled around its average location which advances with a speed slightly less than u_L . These little wrinkles are the reason why u_T is a little larger than u_L .

If $A_0^a = A_0$, Eqs (3.4) and (3.7) can be combined to give a result valid for short times and for any velocity field $u(x, t)$:

$$u_M u_T = u_L^2 + \frac{u_L}{A_0} \int_S u_x dS. \quad (3.9)$$

From the above discussion one can therefore imagine the situation $u_M \approx u_T > u_L$ to be *a priori* plausible at short times predominantly when $\langle u^2 \rangle^{1/2}$ is of the same order as u_L .

4 A FLAMELET IN AN ARBITRARY 1-d VELOCITY FIELD

We now look at the specific problem of a flame sheet in a 1-dimensional velocity field. The flamelet sheet will be described by a line that is convected in the x - y plane by the velocity field and that also moves normal to itself with a constant speed u_L . The velocity field $u(x, t)$ is such that:

$$u(x, t) = [0, v(x, t), 0] \quad (4.1)$$

and the line describing the flame sheet will initially be at $y = 0$ (see Figure 8).

It can be advantageous to approach such a problem from the point of view of a field equation like Eq. (2.4). Ashurst *et al.* (1988) have already done so for a 1-dimensional sinusoidal velocity field in a study of the sensitivity of cusp-formation to the time dependence of the flow. In the present context Eq. (2.4) writes

$$\frac{\partial}{\partial t} G + v(x, t) \frac{\partial}{\partial y} G = u_L |\nabla G|. \quad (4.2)$$

Because the velocity field is 1-dimensional, one expects the line representing the flame sheet to be described at all times by a single valued function $y = y(x, t)$. The solution to Eq. (4.2) should therefore be of the form

$$G(x, y, t) = h(x, t) - y, \quad (4.3)$$

and the initial condition becomes $h(x, t = 0) = 0$. G is now a continuous function

of space—unlike the Heaviside type of solution used in Section 3 to derive Eqs. (3.3) and (3.5), but indeed the kind of function for which Kerstein *et al.* (1988) have shown Eq. (3.6) to be valid—and the flame sheet is represented by the iso-line $G = 0$.

The evolution of $h(x, t)$ is governed by

$$\frac{\partial}{\partial t} h - v(x, t) = u_L \sqrt{1 + \left(\frac{\partial h}{\partial x}\right)^2}. \quad (4.4)$$

We have repeatedly said that an equation like Eq. (2.4), and therefore like Eq. (4.4), leads to irregularities in its solutions—cusps—in finite time, which means that points appear where $\partial h/\partial x$ is discontinuous (Osher and Sethian, 1988). Equations (2.4), (4.2) and (4.4) break down then, but only at those points where these discontinuities arise. One can still safely follow the evolution of h as prescribed by Eq. (4.4) on all the other points of the x - y plane, and trust that in those regions $u = h(x, t)$ does indeed describe the shape of the flame sheet at all times. This model problem will illustrate the differences in the propagation of a flame sheet before and after cusps have had time to form on the sheet. We will find two different relations between u_M and u_T , one valid for short times and the other valid for asymptotically large times; that will help us appreciate how important the presence of cusps is for u_M and u_T to be identical, even though cusps are the reason for the flamelet to be asymmetric about its mean location at large times, and that asymmetry of the flamelet is at short times the reason why $u_M < u_T$.

4.1 The Case $t \gg t_{cusp}$

The flame sheet will soon look like in Figure 8, with $x_{c1}, x_{c2}, x_{c3}, \dots$ being the locations of the cusps. Between any two of those cusps, x_{cj} and x_{cj+1} , the evolution of Eq. (4.4) may be followed, and if the velocity field is stationary, one expects the flame sheet to asymptotically acquire a steady shape (see Ashurst *et al.*, 1988), *i.e.*:

$$h(x, t) = \bar{u}t + H(x), \quad (4.5)$$

where \bar{u} is a constant and can be shown to be equal to $u_T + \langle v \rangle$, whilst H is given by

$$\bar{u} - v(x) = u_L \sqrt{1 + \left(\frac{\partial}{\partial x} H\right)^2}. \quad (4.6)$$

To show that $\bar{u} = u_T + \langle v \rangle$ one can use either Eqs. (3.6) or (3.4). Use of Eq. (3.6) is straightforward, as it only requires a direct integration over space of Eq. (4.6) to give the answer. Use of Eq. (3.4) is not so direct, but more instructive because it will clarify the geometrical meaning of Eq. (4.6).

The angle $\Psi(x)$ that the normal to an iso-line $F = \text{Const.}$ at x makes with the y -axis is such $\partial H/\partial x = \tan \Psi(x)$. Equation (4.6) can therefore be rewritten in the following way:

$$\bar{u} = v(x) + \frac{u_L}{\cos \Psi(x)}. \quad (4.7)$$

From Eq. (4.5), \bar{u} is obviously the speed with which the steady shaped iso-lines

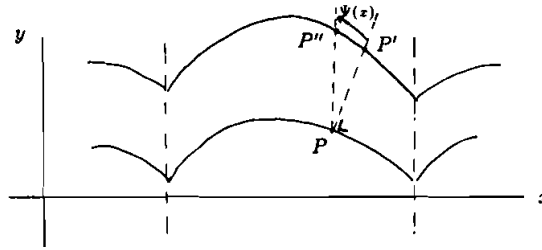


FIGURE 9 The point P on the iso-line at time t moves towards P' at time $t + \delta t$, but the iso-line moves from P to P'' , which is a distance equal to $v(x)\delta t + u_L\delta t/\cos \Psi(x)$. The difference of y -coordinates between P and P' is $v(x)\delta t + u_L \cos \Psi(x)\delta t$.

advance towards the y direction, and therefore the speed u_M of the average location of the iso-line as well. One does indeed expect \bar{u} to be a linear combination of the velocity field $v(x)$, and of the laminar speed "towards" the y direction as given by $u_L/\cos \Psi(x)$ and not $u_L \cos \Psi(x)$! The reason for that (see Figure 9), is that following an iso-line move *after all its possible cusps have formed* is not the same as following a particular point of a given iso-line move. In Figure 9, whilst P moves towards P' , the motion of the iso-line is characterised by the distance between P and P'' and the time it takes for the iso-line crossing P at a given time to then cross P'' . For an infinitesimal time δt , that distance is $v(x)\delta t + u_L\delta t/\cos \Psi(x)$ which is another way of obtaining Eq. (4.7) intuitively. In the meantime P has moved to P' and its y coordinate has increased by $v(x)\delta t + u_L \cos \Psi(x)\delta t$. If there were no cusps on the flamelet, P' would have remained on the same iso-line, and the speed of the advancement of the average location of the flamelet would have been obtained by integrating $v(x) + u_L \cos \Psi(x)$ over all points P on the surface S —see Eq. (3.3). This is of course out of the question when $t \gg t_{\text{cusps}}$, in which case an integration over the whole space of Eq. (4.7) leads to*

$$\bar{u} = \langle v \rangle + \frac{u_L}{\int dx} \int \frac{dx}{\cos \Psi(x)}, \quad (4.8)$$

where $\int dx/\cos \Psi(x)$ is the length L of the iso-line when it has finally reached its equilibrium shape, and $L_0 = \int dx$ is the length of the same iso-line at time $t = 0$, when all iso-lines were straight lines.

$$\bar{u} = \langle v \rangle + \frac{u_L L}{L_0}. \quad (4.9)$$

Replacing in Eq. (3.4) L for A and L_0 for A_0 , we obtain

$$\bar{u} = \langle v \rangle + u_T. \quad (4.10)$$

Equations (4.7) and (4.10) give the shape of the front provided u_T is known and inversely. They can be generalised for a non-stationary velocity field $v(x, t)$ and a

*What we mean by $\int dx$ is $\sum_j \int_{x_j}^{x_{j+1}} dx$. That way we integrate over the whole space by avoiding the points where the cusps lie, thus restricting the integration in those regions where Eqs (2.4), (4.2) and (4.4) are solvable for all times.

flame sheet whose shape has not reached equilibrium yet, but after all possible cusps have formed on the interface [that is crucial in order to deduce Eq. (4.12)]. \bar{u} becomes then a function of x and t , so that

$$\bar{u}(x, t) = v(x, t) + \frac{u_L}{\cos \Psi(x, t)} \quad (4.11)$$

and $u_M(t)$ is now the average value $1/L_0 \int \bar{u}(x, t) dx$, so that

$$u_M(t) = \langle v \rangle_t + u_T(t). \quad (4.12)$$

where \bar{u} is not defined as in Eq. (4.5) anymore, but rather by

$$\frac{\partial h}{\partial t}(x, t) = \bar{u}(x, t). \quad (4.13)$$

4.2 The Case $t \ll t_{cusp}$

For times smaller than t_{cusp} one can apply formula (3.9), which in the present case writes as follows:

$$u_M u_T = u_L^2 + \frac{u_L}{L_0} \oint v dl \quad (4.14)$$

where $\oint dl$ is an integral over the curve that is defined by the iso-line $G = 0$ (or equivalently by the flame sheet), and can be transformed to an integral over x ;

$$u_M(t) u_T(t) = u_L^2 + \frac{u_L}{L_0} \int \frac{v(x, t)}{\cos \Psi(x, t)} dx. \quad (4.15)$$

This formula is valid at short times for any velocity field provided it is 1-dimensional. At times much shorter than t_{cusp} , when the flamelet is still very slightly wrinkled, one can approximate $\cos \Psi(x, t) \approx 1 - \frac{1}{2} \Psi^2(x, t)$, and obtain by a first order expansion in Ψ^2 of Eqs. (4.15) and (3.4) (where $L(t)$ replaces $A(t)$ and L_0 replaces A_0) respectively

$$u_M(t) u_T(t) \approx u_L^2 + u_L \langle v \rangle_t + \frac{u_L}{2L_0} \int v(x, t) \Psi^2(x, t) dx \quad (4.16)$$

and

$$u_T(t) \approx u_L + \frac{u_L}{2L_0} \int \Psi^2(x, t) dx. \quad (4.17)$$

Introducing Eq. (4.17) into Eq. (4.16), a further first order expansion in Ψ^2 gives

$$u_M(t) \approx u_L + \langle v \rangle_t + \frac{1}{2L_0} \int \Psi^2(x, t) [v(x, t) - u_L - \langle v \rangle_t] dx \quad (4.18)$$

It is clear from Eqs (4.17) and (4.18) (particularly in the absence of mean flow, *i.e.* $\langle v \rangle = 0$) when the turbulence is weak compared to u_L (in particular when $v(x, t) \ll$

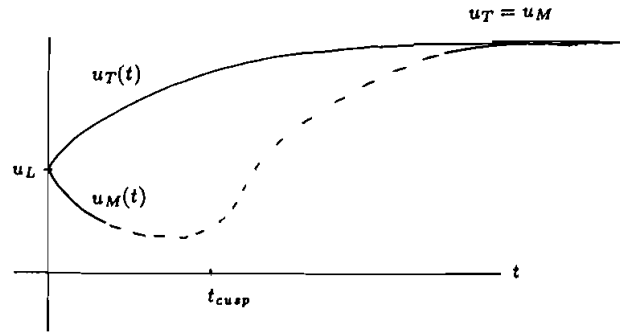


FIGURE 10 The turbulent burning speed u_T and the rate of advancement u_M of the average position of a 1-dimensional flamelet in a 1-dimensional velocity field as functions of time. In this Figure the velocity field is assumed to be stationary and such that $\langle v \rangle_t = 0$ (no mean flow). In that case u_T is a constant when $t \rightarrow +\infty$ (see 4.11). The dashed line corresponds to the behaviour of the flamelet and of u_M around $t \approx t_{\text{cusp}}$ which cannot be reached by our asymptotic analysis.

u_L for all x), that the larger u_T is above u_L because of the turbulence, the smaller u_M is below u_L , as came out in Section 3 for the extreme cases of strong and weak turbulence (in comparison with u_L) and for a larger class of flows than that leading to Eq. (4.16)

4.3 The Global Picture

Figure 10 summarises the global picture concerning the behaviour of u_M with comparison to u_L and u_T that is obtained from the two asymptotic results of sections 4.1 and 4.2 when the turbulence is weak compared to u_L . For simplicity Figure 10 is drawn assuming no average flow, i.e., $\langle v \rangle_t = 0$. For short times $t \ll t_{\text{cusp}}$, u_M is smaller than u_L , whereas u_T is already larger than u_L . u_T may continue to grow above u_L after $t = t_{\text{cusp}}$ because its growth is directly linked to that of the length of the 1-dimensional flamelet, and u_M is asymptotically equal to u_T for $t \gg t_{\text{cusp}}$. Our analysis does not tell us what happens in between these limits, around $t \approx t_{\text{cusp}}$, but the two asymptotic behaviors of u_M that this analysis can reach are valid for both steady and unsteady 1-dimensional velocity fields.

What causes the average position of the flamelet to accelerate and u_M to eventually grow towards $u_M = u_T$ is the formation of cusps on the interface.

An interesting detail of Figure 10 is the behaviour of the two curves $u_M(t)$ and $u_T(t)$ at $t = 0$. One can show that $du_T/dt(t = 0)$ and $du_M/dt(t = 0)$ are both not equal to 0, and must therefore be respectively strictly positive and strictly negative because $u_M = u_L = u_T$ when $t = 0$ and $u_M < u_L < u_T$ when $t > 0$.

From Eq. (4.17),

$$\frac{du_T}{dt}(t = 0) = \frac{u_L}{2L_0} \int \frac{\partial}{\partial t} \Psi^2(x, t = 0) dx, \quad (4.19)$$

and from Eq. (4.18) (assuming $\langle v \rangle_t = 0$),

$$\frac{du_M}{dt}(t = 0) = \frac{1}{2L_0} \int \frac{\partial}{\partial t} \Psi^2(x, t = 0) [v(x, 0) - u_L] dx. \quad (4.20)$$

It is a consequence of Eq. (4.4) that $(\partial/\partial t) \tan \Psi(x, t = 0) = (\partial/\partial x)v(x, 0)$ at \tan

$\Psi(x, t) = (\partial/\partial x)h(x, t)$. Therefore, unless the velocity field is trivial, $(\partial/\partial t)\Psi(x, t = 0) \neq 0$ and the above expressions (4.19) and (4.20) do not vanish. This proves the point we made.

5 NUMERICAL SIMULATION OF A FLAMELET IN 2-d FROZEN TURBULENCE

We simulate 2-dimensional incompressible turbulence by directly summing up random Fourier modes:

$$\mathbf{u}(x, t) = 2\pi \sum_{n=1}^{60} \Delta k_n k_n [\mathbf{v}_n \cos(\mathbf{k}_n \cdot \mathbf{x} + \omega_n t) + \mathbf{w}_n \sin(\mathbf{k}_n \cdot \mathbf{x} + \omega_n t)], \quad (5.1)$$

$$k_{60} = 1, \quad k_1 = 100, \quad k_n = \frac{1 + k_{n-1}}{2}, \quad 2 \leq n \leq 59,$$

$$\Delta k_1 = \frac{k_1 - k_2}{2}, \quad \Delta k_{60} = \frac{k_{59} - k_{60}}{2}, \quad \Delta k_n = \frac{k_{n-1} - k_{n+1}}{2}, \quad 2 \leq n \leq 59.$$

Incompressibility is guaranteed if

$$\mathbf{v}_n \cdot \mathbf{k}_n = \mathbf{w}_n \cdot \mathbf{k}_n = 0 \quad (5.2)$$

and the orientations of the 60 vectors \mathbf{k}_n are chosen from a uniform distribution of all directions and orientations. That determines the directions of \mathbf{v}_n and \mathbf{w}_n , but not their orientations, which we pick at random from another uniform distribution. The amplitudes $v_n = w_n$ are chosen such that the energy spectrum $E(k)$ has the form

$$E(k) \sim k^{-n}. \quad (5.3)$$

We adopt a form (5.3) for the spectrum in the entire range of wavenumbers k used in the simulation, and we conduct experiments with $\omega_n = 0$ so that the velocity field is steady. [For more details on the simulation of such kind of velocity fields see Vassilicos (1990) and Fung *et al.* (1992).]

The flamelet will be simulated by a line typically made of 1000 points. That line will be both advected by the velocity field (5.1) and move normal to itself relative to the fluid. If $u_L = 0$, then the line should never intersect itself because of the incompressibility of the velocity field. When $u_L \neq 0$, cusps may form on a flamelet, but numerically the simulated line starts crossing over itself at those points where they appear, until a loop forms which is not representative of anything real on a flamelet interface (see Figure 1d). Therefore a special ad hoc treatment is needed.

A test case was considered of a line initially square shaped moving inwards with a constant speed u_L , and without any velocity field advecting it. The motion of the line is normal to itself; the tangent to the line at a given point P is defined by taking the direction formed by the two neighbouring points of P on the line, and the normal is of course perpendicular to that direction. The corners of the square immediately developed small square loops outside the main square line that was ‘‘combusting’’ inwards (*i.e.*, moving inwards) (as in Figure 1d, with the difference that the line is initially square rather than curved). This also happened immediately after initial release of the square line when the velocity field (Eq. 5.1) was ‘‘turned on’’ and the

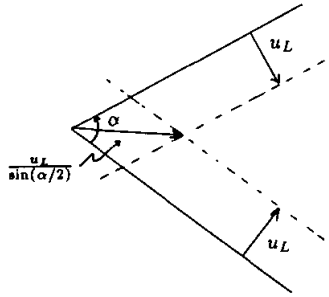


FIGURE 11 The advancement of a flamelet interface at a cusp (where a normal vector cannot be defined) is similar to the advancement of the point intersection of the two blades of a cisor. α is the angle of the cusp; simple trigonometry applies to show that if the points of the interface neighboring the cusp move at a speed u_L normal to the interface, then the cusp itself moves at a speed $u_L/\sin \alpha/2$.

line was advected as well as self-propagating inwards. A possible *a priori* solution to that problem could be to let the simulation run as it is, and cut off the line any such loops as they form. Ignoring the high numerical cost involved in searching for those loops at every time step in order to delete them, the main problem remains that by doing so one would very quickly lose too many points on the line, and would therefore be left with a very poor resolution of that line. One can easily calculate that if $u_L = 0.1$, the time step $\delta t = 0.01$ and the line is initially square shaped of perimeter 1 and with 250 points on each side, then all the points of the line will be cut off in roughly 70 time steps. As the time scale T_E of the turbulence is going to be generally larger than 1 in these simulations, this is not at all satisfactory.

A real cusp due to combustion moves faster than u_L ! It moves with a speed $u_L/\sin \alpha/2$ where α is the angle of the cusp (see Figure 11). Rather than simulate all points P of the line as moving with a speed u_L normal to the line, we will simulate them as moving with a speed $u_L \sin \alpha/2$ where α is the angle that the two neighbouring points to P on the line form with P . That way, we expect loops not to form as fast because cusps will behave realistically after having formed; in fact we still cut points off the line anytime they come too close together (in comparison to a critical distance that we will discuss in the sequel), but we are able to keep the resolution of the line sufficiently good for times as long as two time scales of the turbulence. For the range of parameters dealt with here this has proven to be enough to prevent cusps from degenerating into loops without preventing cusps from forming at all.

Similarly to Section 3, the numerical values of the quantities u_L , E (the total energy of the turbulence), δx (the separation between two points on the line) and δt (the time step) are subject to certain constraints in order to have a good resolution of the line and of its advection by the turbulent flow. The first is that there should be no crossover between two neighbouring points on the line, *i.e.*, we do not allow the line to cross itself. We therefore require that the average distance travelled by any point P of the line in one time step should be much smaller than the distance between P and its direct neighbours on that line, *i.e.*:

$$(u_L + (2E)^{1/2})\delta t \ll \delta x. \quad (5.4)$$

The second constraint is that the motion of the line should be sensitive to the entire range of length scales involved in the simulated turbulence. That implies that the distance travelled by each point P on the line in one time step should be smaller than

the smallest scale of motion, *i.e.*:

$$(u_L + (2E)^{1/2})\delta t \ll \frac{2\pi}{k_1}. \quad (5.5)$$

Throughout this numerical work we fix the value of the time step $\delta t = 0.005$.

Finally, whenever *any* two points of the line come too close together, *i.e.*, whenever they are at a distance $(u_L + (2E)^{1/2})\delta t$ or less from each other, we cut off all the points of the line that are linked between these two. This amounts to cutting off any pockets of unburned fuel and following only the development of the main flamelet. It also amounts to keeping cusps shaped as cusps without degenerating into loops. In fact, the way our algorithm is designed, cusps tend to flatten themselves (the angle α tends to π) because points move with a speed $u_L \sin \alpha/2$ rather than simply u_L . That is a realistic representation of cusps on a flame.

The disadvantage of this algorithm is that it is very expensive, as a check of the separation between each pair of points on the line must be made at each time step. It certainly is not a competitive algorithm for engineering simulations, but it fulfilled the purpose of illustrating the theory in this paper. Because of the cost, only a few runs have been possible; there are therefore no statistics in the results that will follow, but only the results of a number of realisations of the flow. We present eight runs, the first six being mainly illustrative and designed to test the quality of the simulation. In the last two runs we take measurements of the three lower spatial moments and compare with the qualitative results of Section 2.

In order to check the quality of the numerics we release a closed loop rather than an open line in the flow. That way we can follow the value of the area inside the loop, and check that it remains constant (incompressibility of the flow field) when the loop is only advected by the velocity field (5.1) and does not self-propagate normal to itself ($u_L = 0$). When $u_L \neq 0$ we can then check that Eq. (3.5) is obeyed, which in this context takes the form

$$\frac{dA(t)}{dt} = u_L L(t) \quad (5.6)$$

where $A(t)$ is the area inside the loop and $L(t)$ is the length of the loop at any instant of time.

In the six runs that follow we start with a closed square shaped line that burns inwards (*i.e.*, u_L is oriented inside the square), so that the burned fuel is taken to be on the outer side of the square. The burning is chosen to proceed inwards so that the resolution of the line is not lost too early. As the line evolves, cusps and small loops form which our algorithm deals with by cutting off points. There is therefore a decreasing number of points constituting the line with time (there are initially 1000 points), and one is therefore bound to keep a better resolution of the closed line if it “burns” inwards than if it burns outwards.

We start with a square in order to check whether the algorithm can smooth out discontinuities in slope (the corners of the square), without generating cross-overs. In other places of the line we will note that cusps appear, and that the algorithm deals with them successfully as well.

We perform two runs for each realisation of the flow; one with $u_L = 0$ and one with $u_L \neq 0$. As $k_{60} = 1$, the integral length scale of the simulated turbulence is also close to 1 (see Vassilicos 1990); in the first realisation we release a square line of side length 1, so that the line spans a large portion of the flow. The initial separation between the

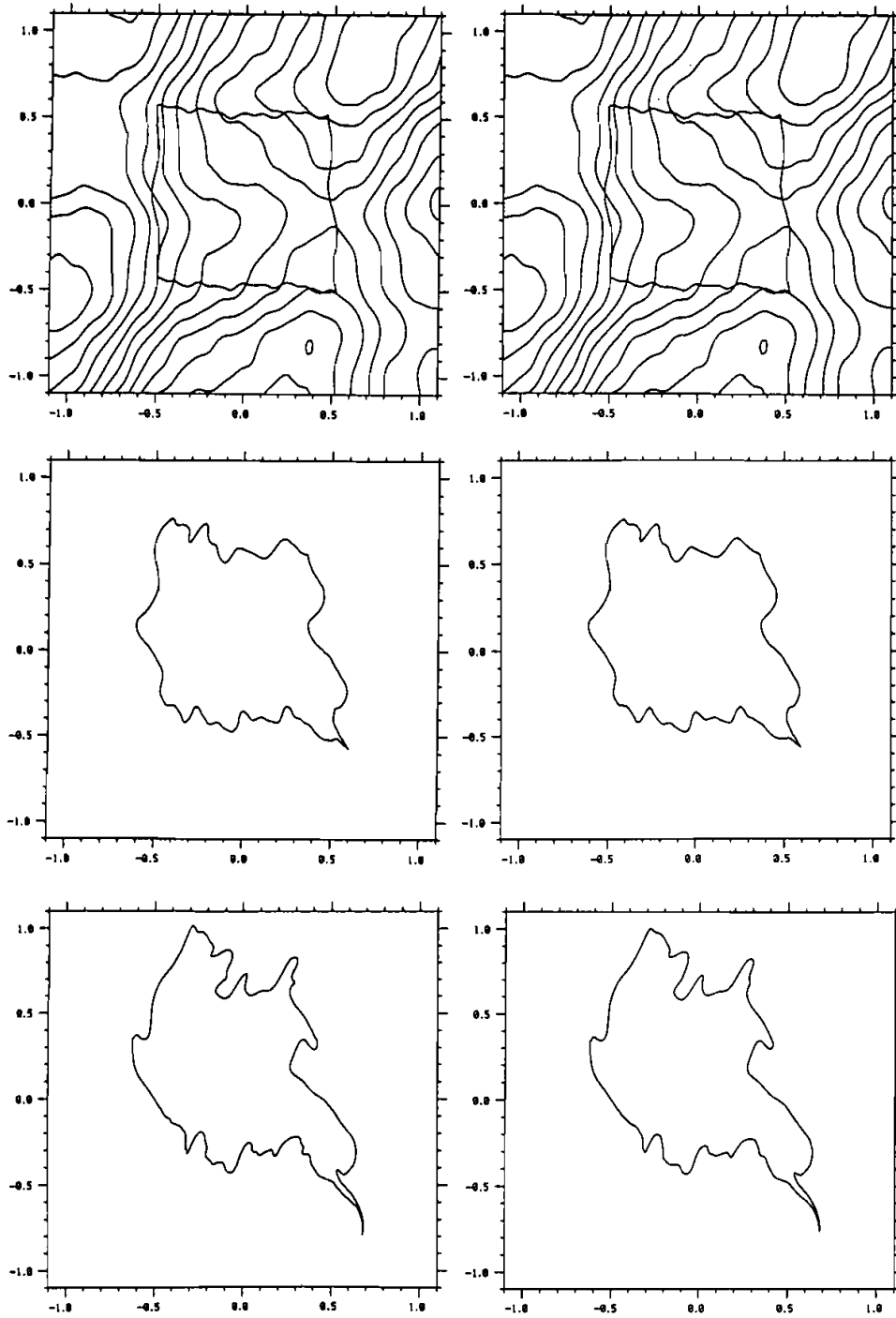


FIGURE 12 $\mu_L = 0$ on the left hand side and $\mu_L = 0.01$ on the right hand side of the page. The side length of the initial square is 1.0. The times are, consecutively, $t = 0.1, 0.4, 0.8$ and 1.0 (on the next page). The time unit is $T_E = 1$.

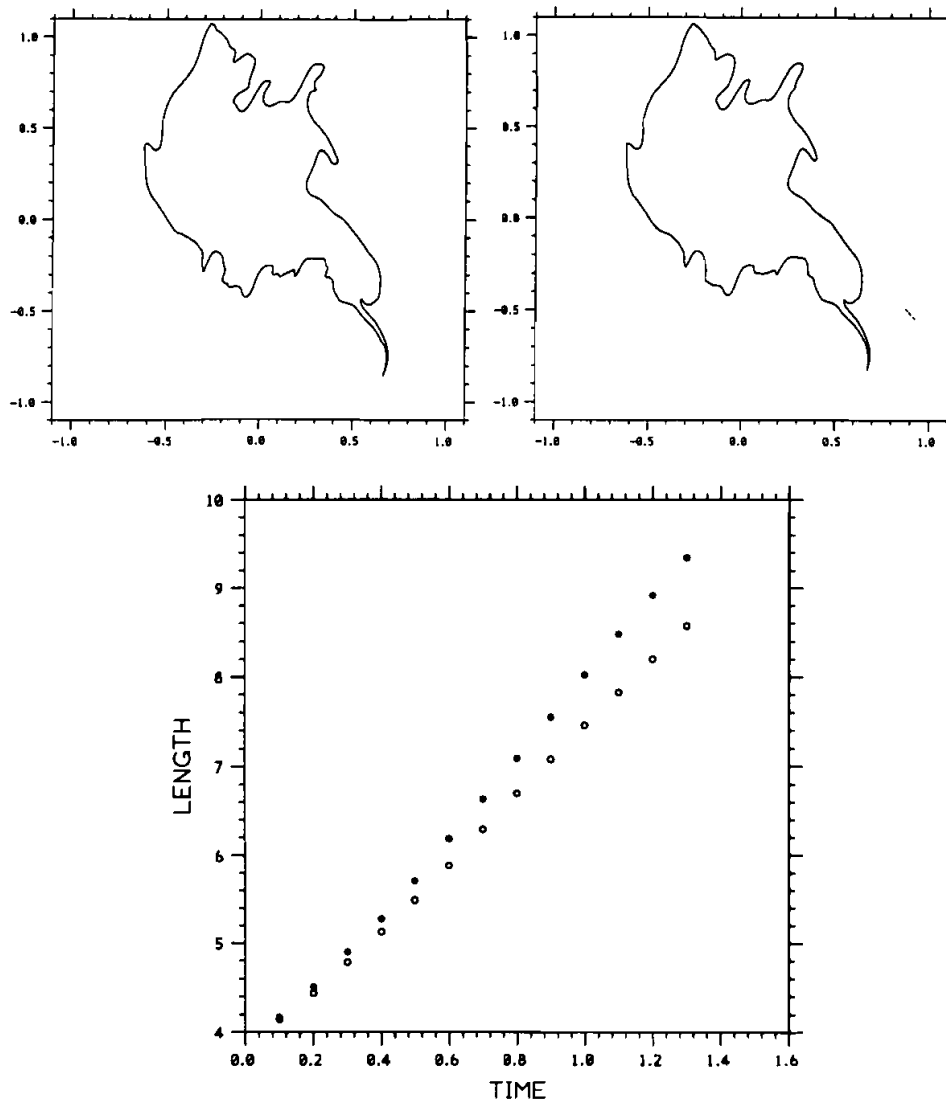


FIGURE 13 The growth of the line with (O) and without (*) combustion. This plot corresponds to the case of Figure 12.

points constituting the line is $\delta x = 4/1000 = 0.004$ (there are 1000 points equally distributed on the four sides of the square). We chose a spectrum (5.3) with $n = 3$ and the values $E = 0.01$ and $u_L = 0$ or 0.01 . These values are consistent with the requirements (5.4) and (5.5), and they lie in the regime of strong turbulence in comparison to u_L , as the intensity of the turbulent fluctuations are of the order $(2E)^{1/2} \approx 0.1$ which is larger than $u_L = 0.01$ by an order of magnitude.

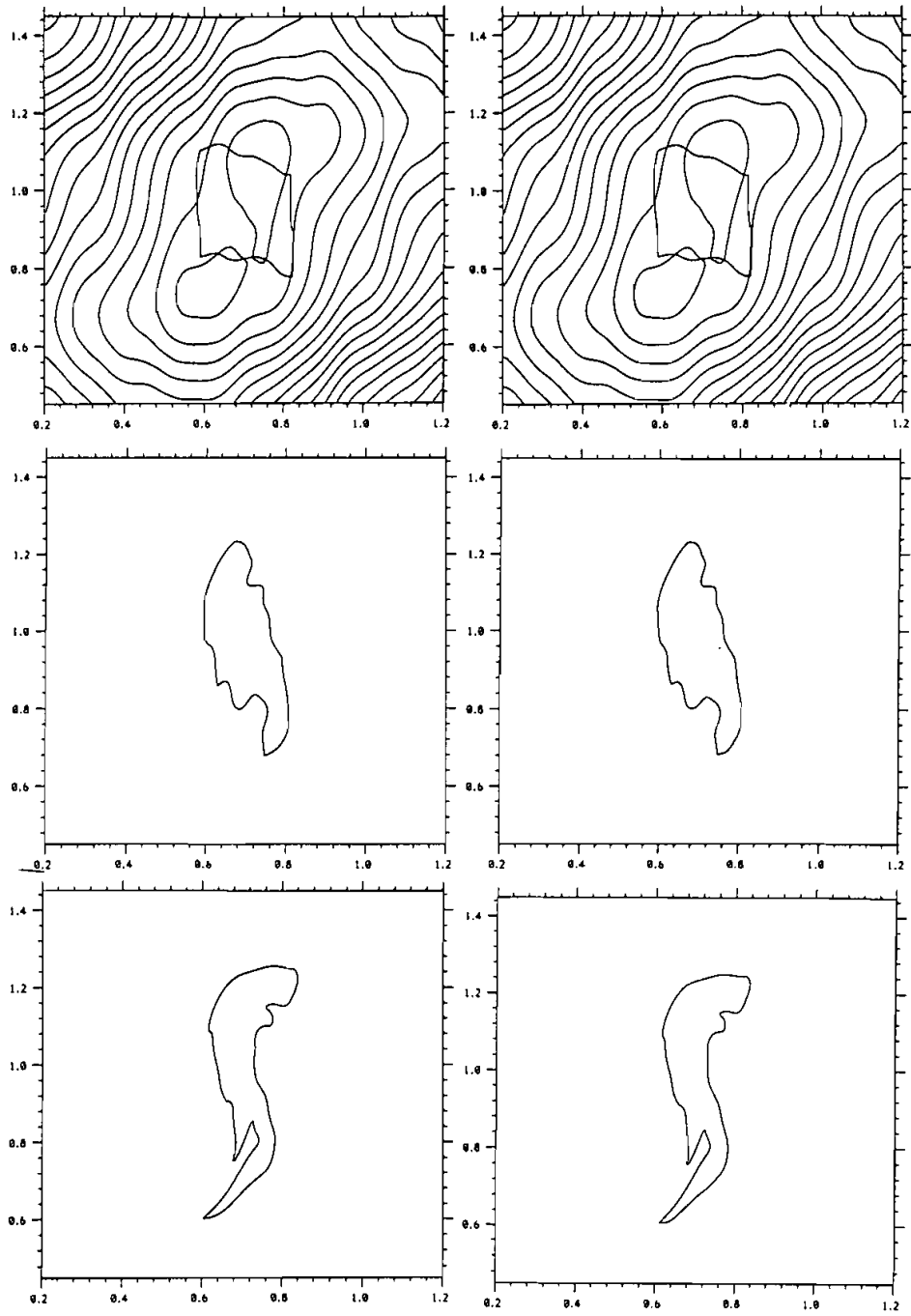


FIGURE 14 $u_L = 0$ on the left hand side and $u_L = 0.01$ on the right hand side of the page. The side length of the initial square is 0.25. The times are, consecutively, $t = 0.01, 0.4, 0.8$ and on the next page, 1.2, 1.5. The time unit is $T_E = 1$.

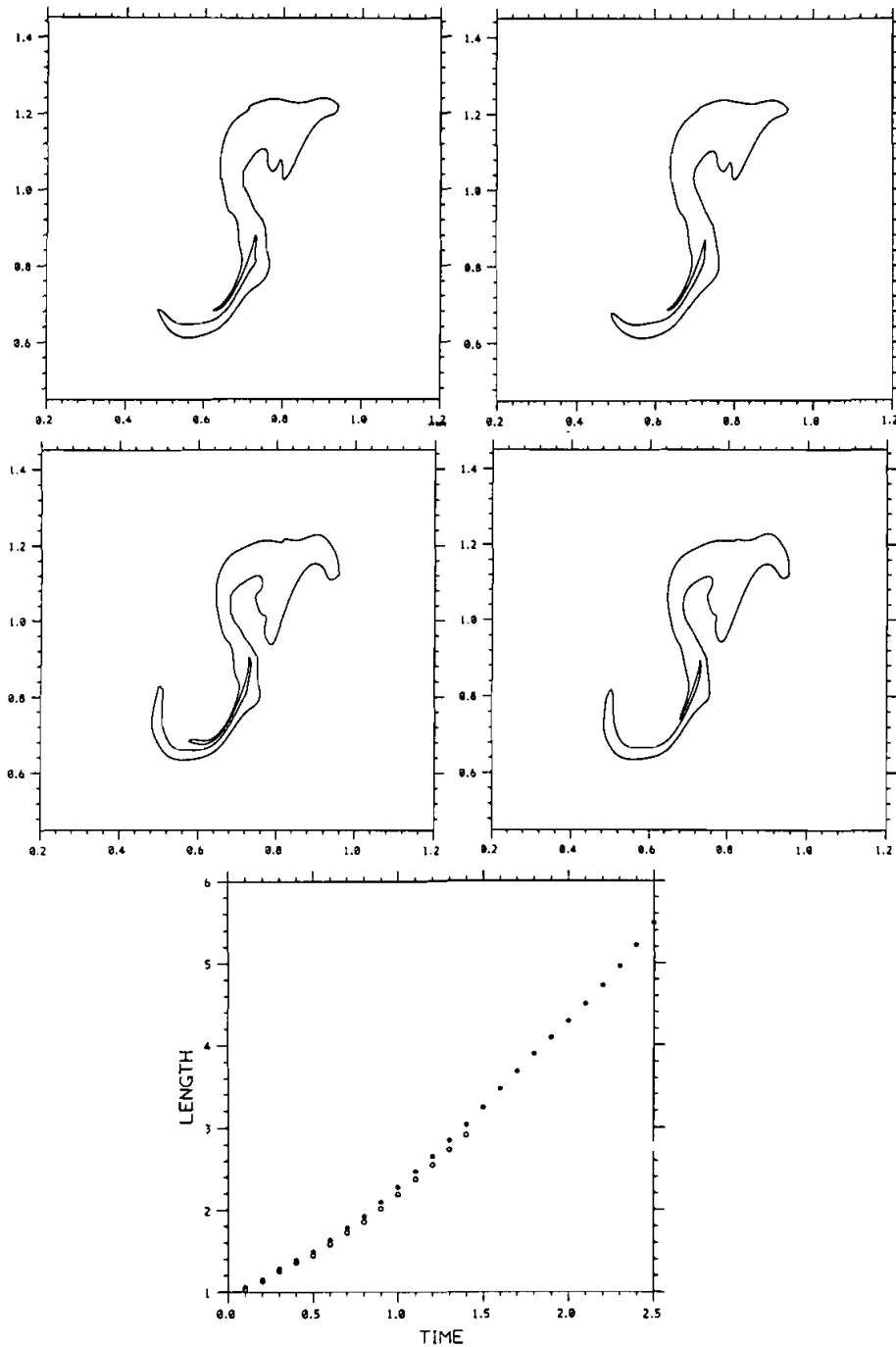


FIGURE 15 Line growth with (O) and without (*) combustion. This plot corresponds to the case of Figure 14.

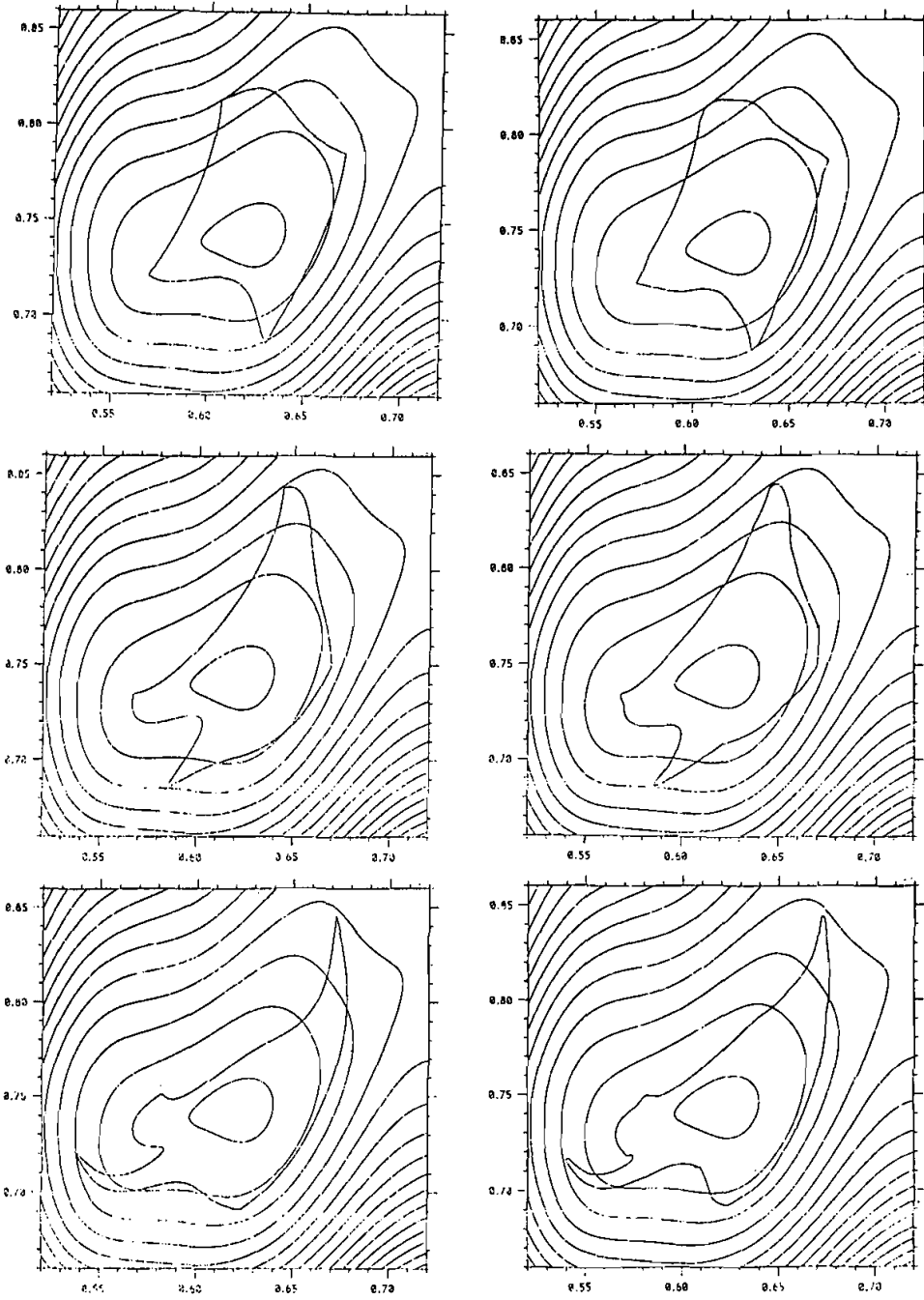


FIGURE 16 $u_L = 0$ on the left hand side and $u_L = 0.01$ on the right hand side of the page. The side length of the initial square is 0.1. The times are, consecutively, $t = 0.1, 0.5, 0.9$ and on the next page, 1.2, 1.6, 1.8, 2.2. The time unit is $T_E = 1$.

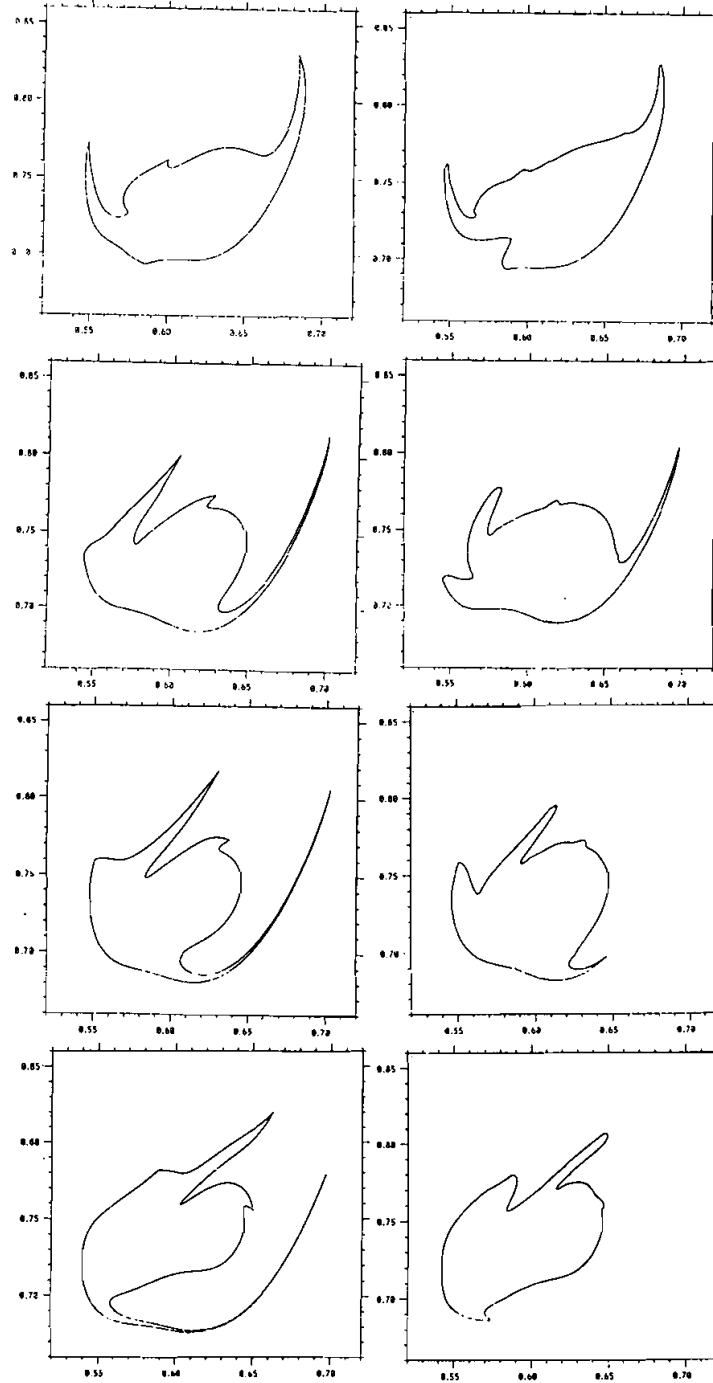


FIGURE 16 Continued.

Figure 12 shows a visual comparison of the development of the line when $u_L = 0$ and when $u_L = 0.01$ in a background of streamlines of the frozen velocity field. The burning and disappearance of convolutions of the flame is clearly visible, as they persist when they are simply filaments of passive dye (the case $u_L = 0$).

In Figure 13 we plot the length of the line with respect to time. It is clear that the growth of that length is faster when $u_L = 0$ than when $u_L = 0.01$.

The next couple of runs are done with the same values of E , u_L and $n = 3$ but in a different region (and realisation) of the flow field. We look at smaller scales, and we start with a square of side length 0.25, which means that initially $\delta x = 1/1000 = 0.001$. The closed line is initially placed between two eddy regions (for a definition of eddy, convergence and streaming regions see Wray and Hunt, 1990) and is therefore trapped in two rotating motions. Figure 14 show the visual comparison of the evolution of the interface for $u_L = 0$ and $u_L = 0.01$. Figure 15 plot the lengths, and the same conclusions can be drawn as for the previous case, in particular that the length of the interface grows faster for a passive interface than for a flamelet; also note the disappearance of long stretched filaments of flame.

The following couple of runs may illustrate burning in a vortex. We now look at even smaller scales than before; the length of a side of the initial square is 0.1 (and therefore $\delta x = 0.0004$ initially), and the square is placed in one eddy region of the flow. The energy spectrum chosen for this couple of runs is steeper than before, *i.e.*, $n = 4$. The results are shown in Figure 16. Of interest in this particular couple of runs is the appearance of a cusp in the case $u_L = 0.01$ at a place of the interface where no cusp appears for the corresponding run with $u_L = 0$.

The two final runs are done for the case where the turbulence is weak in comparison to u_L . We chose $E = 0.0001$ [$(2E)^{1/2} = 0.01$] and $u_L = 0.1$ or 0. Also, we adopt a power $-n = -3$ for the spectrum (5.3). The initial configuration of the line is a circle this time, of initial radius $R = 1$. The separation between points on the line is therefore $\delta x = 2\pi/1000$ initially. We let the simulation run for approximately a bit less than 300 time steps, and we follow the development in time of the average radius, the dispersion and the skewness of the interface (the second and third spatial moments). It is clear from the visualisations of the interface at consecutive times (Figures 17) that the wrinkles on the interface have a larger amplitude when $u_L = 0$ than when $u_L = 0.1$. That is corroborated in Figure 18 where the dispersion is plotted versus time, and where it is clear that the dispersion of a flamelet is larger than the one of a material interface. A related result is that the length of the line grows faster when $u_L = 0$ than when $u_L = 0.1$ (see Figure 19). We also find that for short times the radius of the line decreases less fast than if it was only self-propagating without the action of the velocity field (Eq. 5.1) (see Figure 20). That is in agreement with the theoretical results of the previous sections. Presumably, enough cusps have not had time to form yet on the simulated flamelet. Finally, related to this is the result that the skewness, which remains roughly constant when $u_L = 0$, grows negative when $u_L = 0.1$ (see Figure 21; remember that the burning goes inwards). That is also in agreement with the analysis of Section 2.

6 CONCLUSION

Using Eq. (2.3) from which Williams' field equation (2.4) can be deduced, we have developed a short time formalism that enables one to study the spatial statistics of an

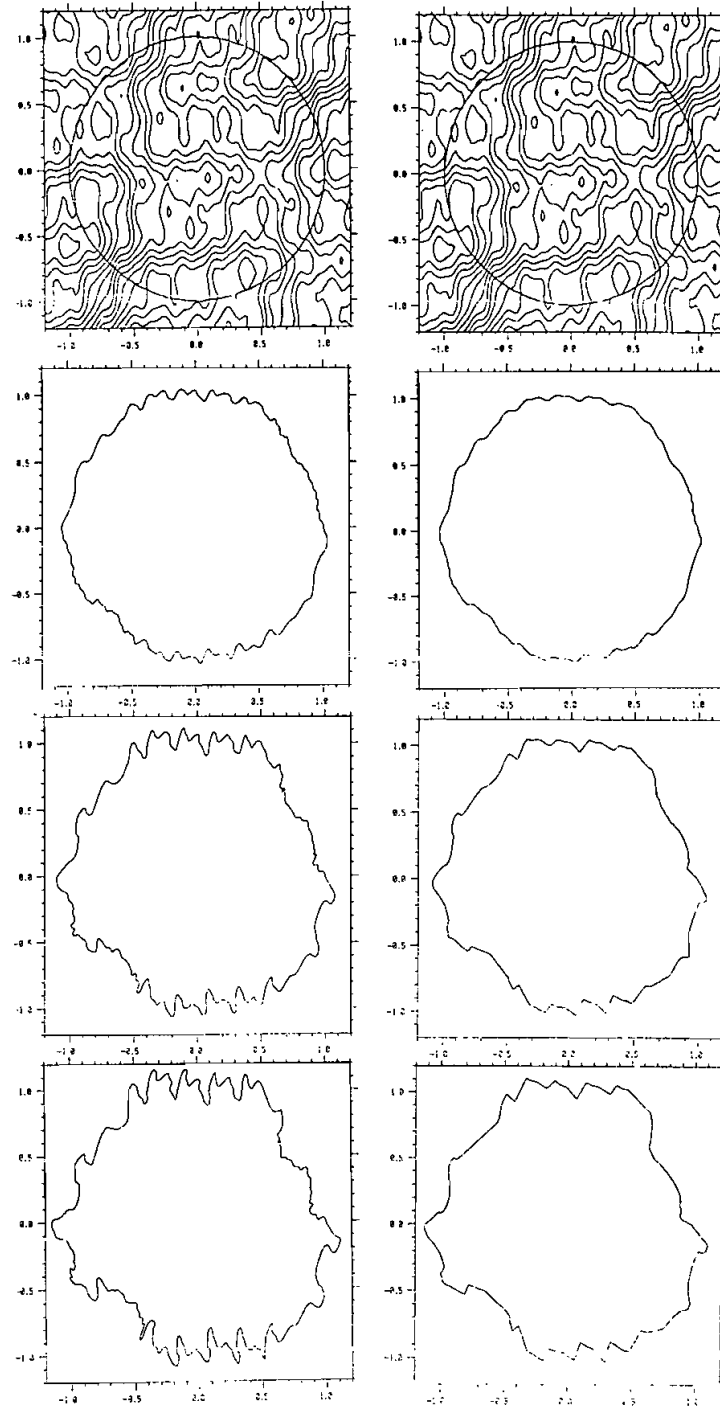


FIGURE 17 $u_L = 0$ on the left hand side and $u_L = 0.1$ on the right hand side of the page. The radius of the initial circle is 1. The times are, consecutively, $t = 0.01, 0.1, 0.2, 0.3$, in time units such that $T_E = 1$.

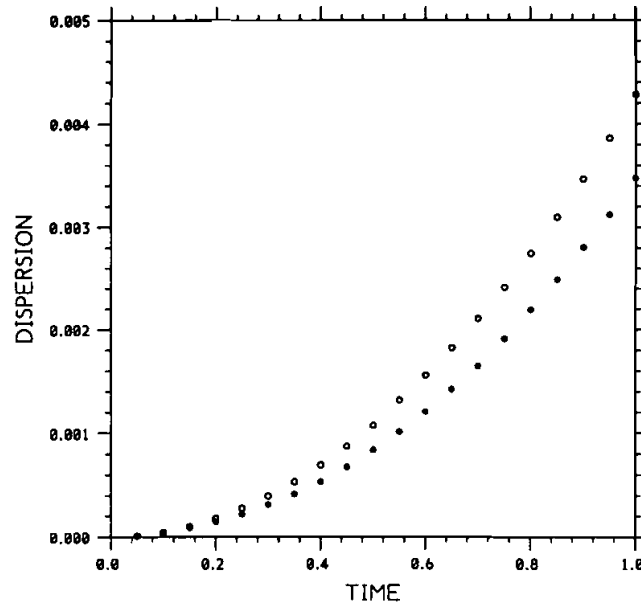


FIGURE 18 Dispersion calculated according to $1/N \sum_{i=1}^N (R_i - \bar{R})^2$ with (●) and without (○) combustion. N is the number of points constituting the curve, R_i is the distance of the i th such point to the centre of the original circle and $\bar{R} = 1/N \sum_{i=1}^N R_i$. This plot corresponds to the case of Figure 17 but the time units are such that $T_E = 10$.

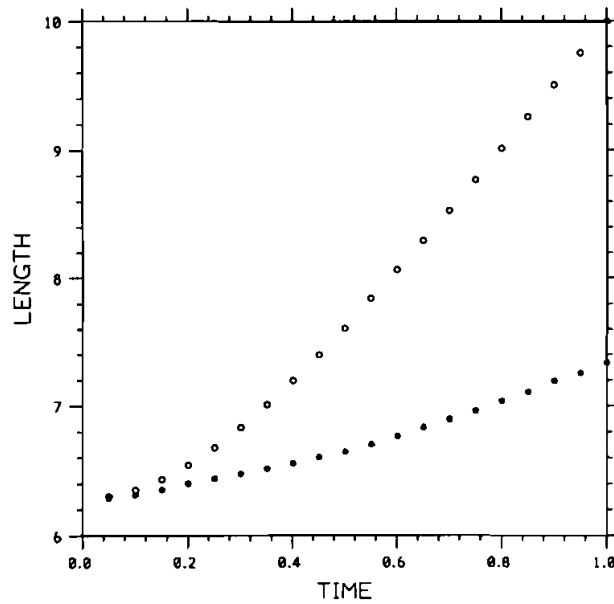


FIGURE 19 Growth of the length of the closed loop. The time units are such that $T_E = 10$.

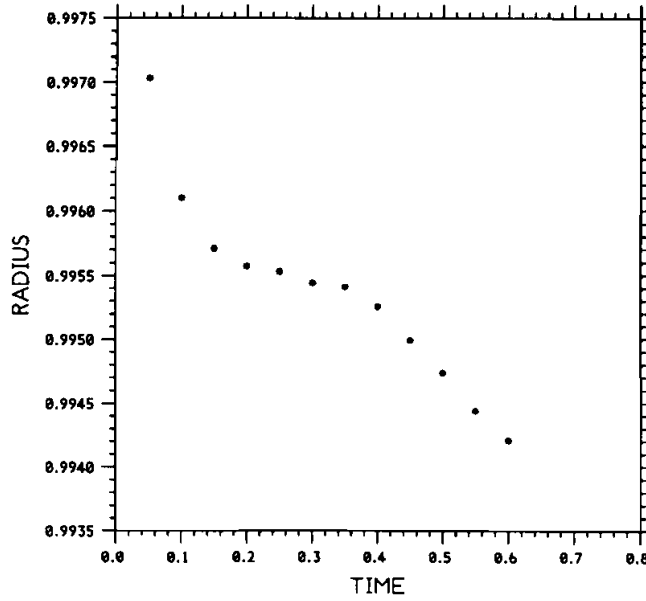


FIGURE 20 The average radius \bar{R} of the loop calculated as shown in Figure caption 18. If there was no turbulence the radius of the imploding circle would have been equal to 0.990 at $t = 0.1$ with the units of this plot which are such that $T_E = 10$.

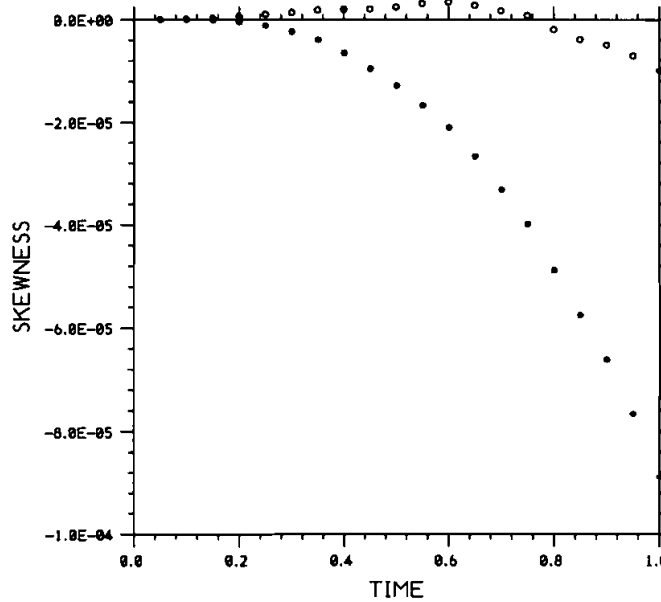


FIGURE 21 The skewness of the deformation of the circle around its mean radius \bar{R} . We calculate it according to $1/N \sum_{i=1}^N (R_i - \bar{R})^3$. The time units are such that $T_E = 10$. (*) with combustion; (O) without combustion.

entire flame sheet (not only flame sheet surface elements) where the density and viscosity difference across the sheet is so small as to have a negligible effect on the flow.

This study is based on a particular class of solutions of Eq. (2.3) that are not solutions of Eq. (2.4). As opposed to analysing the flame sheet as a single thin interface, in this type of solution the flame sheet occupies the space between two interfaces. The average volume between these interfaces is conserved; this makes it possible to define a spatial probability density function F/\bar{V} for the flamelet interface, and thus derive the formalism mentioned above.

The analysis is valid for times much shorter than the time needed for cusps or pockets of unburned fuel to form, and the main results obtained are the following:

(1) If the turbulence is too weak or too strong compared with u_L , the rate of advancement of the average location of the flame front can be shown to be smaller than even the laminar flame speed! This rate of advancement should therefore not be mistaken, in general, for the turbulent burning speed.

(2) Under the same condition regarding the ratio of the turbulent fluctuations to u_L , the dispersion of the flame is increased by the turbulence and reduced by the laminar flame speed u_L . For longer times, combustion should still be reducing the flame's dispersion because of cusps gradually appearing on the interface. The present analysis is nevertheless unable to reach such an effect.

(3) The dispersion of the flame is skewed towards the direction of the flame's propagation unlike the dispersion of a passive contaminant in a homogeneous and isotropic velocity field which does not develop any statistical asymmetry.

The study of a flamelet in an arbitrary 1-dimensional velocity field has shown that for long times (typically much longer than the time needed for cusps to form on the interface), the rate of advancement u_M of the average location of the flamelet is equal to the turbulent burning speed u_T . On the other hand, for times before cusps have formed u_M is appreciably smaller than u_T , and even smaller than u_L . That is caused by the immediate growth of the asymmetry of the flame interface after initial release of the flame, and by the absence of cusps. It is only if cusps do form on the flamelet that $u_M = u_T$ may eventually hold.

Finally we present the results of a 2-dimensional numerical simulation of a flamelet in a turbulent velocity field that support the points (1), (2) and (3) above.

ACKNOWLEDGEMENTS

We are grateful for many fruitful discussions with H. K. Moffatt and N. Peters, and also for the comments of one very careful anonymous referee. JCV acknowledges financial support from an EEC contract ST2J-0029-1-F during the course of this study.

REFERENCES

- Ashurst, W. T., Sivashinsky, G. I., and Yakhot, V. (1988). Flame front propagation in unsteady hydrodynamic fields. *Combust. Sci. Tech.* **62**.
- Batchelor, G. K. (1952). The effect of homogeneous turbulence on material lines and surfaces. *Proc. R. Soc. Lond.* **213**, 349.
- Batchelor, G. K. (1959). Small-scale variation of convected quantities like temperature in turbulent fluid. Part 1. General discussion and the case of small conductivity. *J. Fluid Mech.* **5**, 113.
- Batchelor, G. K. (1967). *An Introduction to Fluid Dynamics*. Cambridge University Press, Cambridge.
- Batchelor, G. K. and Townsend, A. A. (1956). Turbulent diffusion. In G. K. Batchelor & R. M. Davies (Eds) *Surveys in Mechanics*. Cambridge University Press, Cambridge.

- Clavin, P. (1985a). Dynamic behaviour of premixed flame fronts in laminar and turbulent flows. *Prog. Energy Combust. Sci.* **11**, 1.
- Clavin, P. (1985b). Fundamental aspects of premixed flames. In P. Calvin, B. Larrouturou and P. Pelce (eds) *Combustion and Nonlinear Phenomena*. Les Editions de Physiques, Paris.
- Drummond, I. T. and Munch, W. H. P. (1990). Turbulent stretching of line and surface elements. *J. Fluid Mech.* **215**, 45.
- Fung, J. C. H., Hunt, J. C. R., Malik, N. A., and Perkins, R. J. (1992). Kinematic simulation of homogeneous turbulent flows generated by unsteady random fourier modes. *J. Fluid Mech.* **236**, 281.
- Kerstein, A. R., Ashurst, W. T., and Williams, F. A. (1988). Field equation for interface propagation in an unsteady Homogeneous flow field. *Phys. Rev.* **A37**, 2728.
- Lamb, H. (1932). *Hydrodynamics*, 6th edition. Cambridge University Press, Cambridge.
- Landau, L. D., Lifshitz, E.M., (1959) *Fluid Mechanics*. Volume 6 of *Course of Theoretical Physics*. Pergamon Press.
- Markstein, G. H. (1951). Experimental and theoretical studies of flame front stability. *J. Aeronaut. Sci.* **18**, 199.
- Moffatt, H. K. (1987). Unpublished.
- Osher, S. and Sethian, J. A. (1988). Fronts propagating with curvature-dependent speed: Algorithms based on Hamilton–Jacobi formulations. *J. Comp. Phys.* **79**, 12.
- Peters, N. (1986). Laminar flamelet concepts in turbulent combustion. *21st International Symposium on Combustion*, Munich.
- Peters, N. (1987). *Length and Time Scales in Turbulent Combustion*. U.S.–France Workshop on Turbulent Reacting Flow, Rouen, France, July 1987.
- Peters, N., Gottgens, J., Klein, R., and Clavin, P. (1988). *A Model Equation for the Mean Premixed Flame Surface Area*. Preprint, Institute fur Technishe Mechanik, Aachen.
- Pope, S. B. (1987). Turbulent premixed flames. *Ann. Rev. Fluid Mech.* **19**, 237.
- Pope, S. B. (1988). The evolution of surfaces in turbulence. *Int. J. Engng Sci.* **26**, 5.
- Saffman, P. G. (1960). On the effect of the molecular diffusivity in turbulent diffusion. *J. Fluid Mech.* **8**, 273.
- Sethian, J. A. (1985). Curvature and the evolution of fronts. *Commun. Math. Phys.* **101**, 487.
- Sivashinsky, G.I. (1983). Instabilities, patrn formation, and turbulence in flames. *Ann. Rev. Fluid Mech.* **15**, 179.
- Sivashinsky, G. I. (1988). Cascade renormalisation theory of turbulent flame speed. *Combust. Sci. Tech.* **62**, 77.
- Strehlov, R. A. (1984). *Combustion Fundamentals*. McGraw Hill, New York.
- Taylor, G. I. (1921). Diffusion by continuous movements. *Proc. Lond. Math. Soc., ser. 2* **20**, 196.
- Vassilicos, J. C. (1990). Fractal and moving interfaces in turbulent flows. Ph.D. Dissertation, University of Cambridge.
- Williams, F. A. (1985a). *Combustion Theory*, 2nd edition. Benjamin-Cummings, Menlo Park.
- Williams, F. A. (1985b). Turbulent combustion. In J. D. Buckmaster (ed.) *The Mathematics of Combustion* SIAM, Philadelphia.
- Wray, A. A. and Hunt, J. C. R. (1990). Algorithms for classification of turbulent structures. In H. K. Moffatt & A. Tsinober (eds) *Proc. of IUTAM Symp. on Topological Fluid Mechanics*. Cambridge University Press, Cambridge.
- Yakhot, V. (1988). Scale invariant solutions of the theory of thin turbulent flame propagation. *Combust. Sci. Tech.* **62**, 127.

APPENDIX A

In the system of local coordinates (n, s_1, s_2) of an interface where n is the coordinate along the normal and s_1, s_2 are the two tangential coordinates, the equation describing that interfee will be written as:

$$n = v(s_1, s_2) = \text{Const.} \quad (\text{A.1})$$

One can describe the fact that an interface propagates through the turbulent medium due to the combined action of the velocity field and the laminar flame speed

u_F by writing,

$$v(s_1, s_2, t) = v_0(s_1, s_2) + \int_0^t (\mathbf{u} \cdot \mathbf{n} + u_F) d\tau, \quad (\text{A.2})$$

where $\mathbf{u} \cdot \mathbf{n}$ is taken at $[s_1, s_2, v(s_1, s_2, \tau)]$ at time τ .

Then at time t the equation of the interface is

$$n = v(s_1, s_2, t) = \text{Const.}, \quad (\text{A.3})$$

whereas

$$n = v_0(s_1, s_2) = \text{Const.} \quad (\text{A.4})$$

is the equation of the initial configuration of the interface.

We know that the evolution Eqs. (2.3) and (2.4) contain the combined effect of both the turbulence and the laminar flame speed on the propagation of the interface.

One therefore expects the step function

$$F(s_1, s_2, n; t) = H[n - v(s_1, s_2, t)] \quad (\text{A.5})$$

to be solution of both Eqs (2.3) and (2.4) as it is also a monotonic function in n . That can be checked fairly easily:

$$\frac{\partial}{\partial t} F(s_1, s_2, n; t) = -\delta[n - v(s_1, s_2, t)][u_F + \mathbf{u} \cdot \mathbf{n}(t)]$$

$$\mathbf{u} \cdot \nabla F = \mathbf{u} \cdot \mathbf{n} \frac{\partial}{\partial n} H[n - v(s_1, s_2, t)] = \mathbf{u} \cdot \mathbf{n} \delta[n - v(s_1, s_2, t)]$$

$$u_F \mathbf{n} \cdot \nabla F = u_F \delta[n - v(s_1, s_2, t)].$$

Sum up these three equalities and get zero. Hence Eq. (1.5) is indeed a solution of Eq. (2.3), and because it is a monotonous function, it is also solution of Eq. (2.4).

It should be emphasized that this solution holds as long as one can write an expression like Eq. (A.2). That is no longer possible if the surface gets to intersect itself!

Linear combinations of such solutions are also solutions of Eq. (2.3)—but not of Eq. (2.4) in general, unless they happen to be monotonic in n . In other words,

$$F(s_1, s_2, n; t) = \sum_{j=1}^N c_j H[n - v_j(s_1, s_2, t)] + \text{Const.} \quad (\text{A.6})$$

where the $v_j(s_1, s_2, t), j = 1, \dots, N$, describe N interfaces that do not intersect each other nor themselves, is a solutions of Eq. (2.3). ($c_j, j = 1, \dots, N$, are constant coefficients.)

$$v_j(s_1, s_2, t) = v_j^0(s_1, s_2) + \int_0^t u_F d\tau + \int_0^t \mathbf{u} \cdot \mathbf{n}[s_1, s_2, v_j(s_1, s_2, \tau), \tau] dt \quad (\text{A.7b})$$

$$v_j^0(s_1, s_2) = v_j(s_1, s_2, t = 0). \quad (\text{A.7b})$$

In order to check this solution we calculate $(\partial/\partial t) F$, $\mathbf{u} \cdot \nabla F$ and $u_F \mathbf{n} \cdot \nabla F$ as we did before and sum up to obtain:

$$\begin{aligned} \frac{\partial}{\partial t} F + (\mathbf{u} + u_F \mathbf{n}) \cdot \nabla F &= \sum_{j=1}^N c_j \delta[n - v_j(s_1, s_2, t)] \\ &\times [\mathbf{u} \cdot \mathbf{n}(s_1, s_2, n, t) - \mathbf{u} \cdot \mathbf{n}(s_1, s_2, v_j(s_1, s_2, t), t)]. \end{aligned} \quad (\text{A.8})$$

The right-hand side of Eq. (A.8) does indeed vanish when $n \neq v_j(s_1, s_2, t)$ for all $j = 1, \dots, N$, or when there exists only one j such that $n = v_j(s_1, s_2, t)$. Note that if there exists two distinct j and k , $j \neq k$, such that $n = v_j(s_1, s_2, t) = v_k(s_1, s_2, t)$, the right-hand side of Eq. (A.8) does not vanish any longer for that particular value of n . That corresponds to the case when the two interfaces j and k intersect.

We can therefore safely conclude that as long as all interfaces $j = 1, \dots, N$ do not intersect each other nor themselves, Eq. (A.6) is a solution of Eq. (2.3) (but not of Eq. (2.4)!).

APPENDIX B

Suppose $F(x) = \sum_{j=1}^N H(x - x_j)$. Then,

$$\left| \frac{dF}{dx} \right| = \sum_{j=1}^N \delta(x - x_j)$$

and therefore

$$\int_{-\infty}^{+\infty} \left| \frac{dF}{dx} \right| dx = N. \quad (\text{B.1})$$

Equation (B.1) can be generalised in more than one dimensions in the following way (e.g. see Ashurst *et al.*, 1988):

$$\int_{\text{all space}} |\nabla F| dV = S, \quad (\text{B.2})$$

where F is again a function that can only take one of two values 0 or 1 over the whole space, and S is the surface area of the interface that separates regions where $F = 0$ from regions where $F = 1$.

Generalising even further, for any function $g(\mathbf{x})$ one can write,

$$\int_{\text{all space}} g(\mathbf{x}) |\nabla F| dV = \int_S g(\mathbf{x}) dS. \quad (\text{B.3})$$